REPUBLIC OF TURKEY
ISTANBUL GELISIM UNIVERSITY
INSTITUTE OF GRADUATE STUDIES

Department of Electrical-Electronic Engineering

POWER QUALITY ENHANCEMENT USING STATCOM WITH PV SYSTEMS

Master Thesis

Ammar ALHASIRI

Supervisor

Asst. Prof. Dr. Yusuf Gürcan ŞAHİN

Istanbul – 2023

THESIS INTRODUCTION FORM

Name and Surname : Ammar ALHASIRI

Language of the Thesis : English

Name of the Thesis : Power quality enhancement Using STATCOM With PV Systems

Institute : Istanbul Gelisim University Institute of Graduate Studies

Department : Electrical-Electronic Engineering

Thesis Type : Master

Date of the Thesis : 19.07.2023

Page Number : 86

Thesis Supervisors : Asst. Prof. Dr. Yusuf Gürcan ŞAHİN

Index Terms : DSTATCOM, VSC, THD%, PV system.

Turkish Anstract : Doğrusal olmayan yüklerin ve güç faktörlerinin getirdiği harmonikler gibi dağıtım güç sisteminde güç kalitesi sorunları bir problemdir. Senkron jeneratör akımları, harmonikler büyüdükçe bozulur. Bu sorunları ele almak için araştırmacılar tarafından farklı stratejiler kullanılmıştır. En önemli bileşenlerden biri, dağıtım sistemi (DSTATCOM) için statik senkron kompansatördür. Üç ayaklı Gerilim Kaynağı Dönüştürücüsünün (VSC) DSTATCOM dc-link kanalı, senkron jeneratör akımları için Toplam Harmonik Bozulmayı % THD'yi azaltmak üzere bir PV sistem kaynağı (PV panelleri veya piller) tarafından beslenir. PV panellerin ürettiği gerilim değişken olduğu için bu yöntem tamamlanmamış kabul edilir. Ne de olsa, hava

için radyasyon ve sıcaklık değişiminden etkilenir. Ayrıca, bataryanın derin döngüsü sınırlıdır. Bu tezde, bataryalı PV paneller, DSTATCOM'un DC bara gerilimini sağlamak için bir PV sistemi olarak birlikte kullanılmıştır. Kompanzasyon sistemi için birden fazla PV sistemi enerji kaynağı arasındaki güç yönetimini kontrol etmek için oldukça koordineli bir tasarım kullanılır. Üç ayaklı VSC'li DSTATCOM, baraların gerilim değerlerini limitler aralığında tutmak için kullanılır. Çalışmanın simülasyon sonuçları, FV sistem kaynağının, DSTATCOM'un dc-bağlantısının bireysel kaynaklarına kıyasla üstün bir zaman yanıtına sahip olduğunu, üç fazlı akım kaynağının %THD'sini azalttığını göstermektedir.

Distribution List **:** 1. To the Institute of Graduate Studies of Istanbul Gelisim University
2. To the National Thesis Center of YÖK (Higher Education Council)

Ammar ALHASIRI

REPUBLIC OF TURKEY
ISTANBUL GELISIM UNIVERSITY
INSTITUTE OF GRADUATE STUDIES

Department of Electrical-Electronic Engineering

POWER QUALITY ENHANCEMENT USING STATCOM WITH PV SYSTEMS

Master Thesis

Ammar ALHASIRI

Supervisor

Asst. Prof. Dr. Yusuf Gürcan ŞAHİN

Istanbul – 2023

DECLARATION

I hereby declare that in the preparation of this thesis, scientific ethical rules have been followed, the works of other persons have been referenced in accordance with the scientific norms if used, there is no falsification in the used data, any part of the thesis has not been submitted to this university or any other university as another thesis.

Ammar ALHASIRI

…./…./2023

TO ISTANBUL GELISIM UNIVERSITY

THE DIRECTORATE OF GRADUATE EDUCATION INSTITUTE

The thesis study of Ammar Yasir Nadheer ALHASIRI titled as Power quality enhancement Using STATCOM With PV Systems has been accepted as MASTER in the department of Electrical-Electronic Engineering by out jury.

Director _____

Asst. Prof. Dr. Yusuf Gurcan SAHIN

(Supervisor)

Member _____

Asst. Prof. Dr. Sevcan KAHRAMAN

Member _____

Asst. Prof. Dr. Kenan BUYUKATAK

APPROVAL

I approve that the signatures above signatures belong to the aforementioned faculty members.

... / ... / 20..

Prof. Dr. Izzet GUMUS

Director of the Institute

SUMMARY

Power quality problems in the distribution power system such as harmonics brought on by non-linear loads and power factors are a problem. The synchronous generator currents get distorted as harmonics grow. Different strategies have been employed by researchers to address these issues. One of the most crucial components is the static synchronous compensator for the distribution system (DSTATCOM). The DSTATCOM dc-link channel of the Voltage Source Converter (VSC) with three legs is fed by a PV system source (PV panels or batteries) to reduce the Total Harmonic Distortion THD% for synchronous generator currents. This method is considered uncompleted because the generated voltage of PV panels is variable. After all, it is affected by the variation of radiation and temperature for the weather. Also, the deep cycle of the battery is limited. In this thesis, the PV panels with batteries have been used together as a PV system to supply the DC link voltage of DSTATCOM. A highly coordinated design is used to control the power management between multiple PV system energy sources for the compensation system. DSTATCOM with three-legs VSC is used to keep the voltage values of the buses within the limits range. The simulation results of the work show that the PV system source has a superior time response compared with the individual sources of the dc-link of DSTATCOM reduces the THD% of the three phases current source.

Key Words: DSTATCOM, VSC, THD%, PV system.

ÖZET

Doğrusal olmayan yüklerin ve güç faktörlerinin getirdiği harmonikler gibi dağıtım güç sisteminde güç kalitesi sorunları bir problemdir. Senkron jeneratör akımları, harmonikler büyüdükçe bozulur. Bu sorunları ele almak için araştırmacılar tarafından farklı stratejiler kullanılmıştır. En önemli bileşenlerden biri, dağıtım sistemi (DSTATCOM) için statik senkron kompansatördür. Üç ayaklı Gerilim Kaynağı Dönüştürücüsünün (VSC) DSTATCOM dc-link kanalı, senkron jeneratör akımları için Toplam Harmonik Bozulmayı % THD'yi azaltmak üzere bir PV sistem kaynağı (PV panelleri veya piller) tarafından beslenir. PV panellerin ürettiği gerilim değişken olduğu için bu yöntem tamamlanmamış kabul edilir. Ne de olsa, hava için radyasyon ve sıcaklık değişiminden etkilenir. Ayrıca, bataryanın derin döngüsü sınırlıdır. Bu tezde, bataryalı PV paneller, DSTATCOM'un DC bara gerilimini sağlamak için bir PV sistemi olarak birlikte kullanılmıştır. Kompanzasyon sistemi için birden fazla PV sistemi enerji kaynağı arasındaki güç yönetimini kontrol etmek için oldukça koordineli bir tasarım kullanılır. Üç ayaklı VSC'li DSTATCOM, baraların gerilim değerlerini limitler aralığında tutmak için kullanılır. Çalışmanın simülasyon sonuçları, FV sistem kaynağının, DSTATCOM'un dc-bağlantısının bireysel kaynaklarına kıyasla üstün bir zaman yanıtına sahip olduğunu, üç fazlı akım kaynağının %THD'sini azalttığını göstermektedir.

Anahtar Kelimeler: DSTATCOM, VSC, THD%, PV sistemi.

TABLE OF CONTENTS

CHAPTER THREE
DESIGN AND SIMULATION OF DSTATCOM

CHAPTER FOUR
ANALYSIS AND DISCUSSION SIMULATION RESULTS

CONCLUSIONS AND SUGGESTIONS FOR FUTURE WORK

REFERENCES

ABBREDIVATIONS

AC	**:**	Alternating Current
CSC	**:**	Current Source Converter
CV	**:**	Constant Voltage method
DC	**:**	Direct Current
DSTATCOM	**:**	Distribution Static Synchronous Compensator
IGBT	**:**	Isolated Gate Bipolar Transistor
INC	**:**	Incremental Conductance method
ISPT	**:**	Instant Symmetrical Part theory
MOSFET	**:**	Metal Oxide Semiconductor Field-Effect Transistor
MP	**:**	Maximum Power
MPP	**:**	Maximum Power Point
MPPT	**:**	Maximum Power Point Tracking
OCV	**:**	Open Circuit Voltage method
OLF	**:**	Over load factor
PBT	**:**	Power Balance Theory
PCC	**:**	Point of Common Coupling
PI	**:**	Proportional-Integral
PLL	**:**	Phase Locked Loop
P&O	**:**	Perturb Observe method
PQ	**:**	Power Quality
PSO	**:**	Particle Swarm Optimization Algorithm
PV	**:**	Photovoltaic
PWM	**:**	Pulse Width Modulation
SCC	**:**	Short Circuit Current method
STATCOM	**:**	Static Synchronous Compensator
SVC	**:**	Static Var Compensator
SRFM	**:**	Synchronous Reference Frame Method
SRFMUV	**:**	Synchronous Reference Frame Method with Unit Vector

TCR	**:**	Thyristor Controller Rectifier
THD	**:**	Total Harmonic Distortion
Vbus	**:**	Voltage of the bus
VSC	**:**	Voltage Source Converter

LIST OF TABLES

LIST OF FIGURES

INTRODUCTION

The main aim of the electrical power system is to generate, transfer, and distribute active and reactive power with different types of loads connected to the power system. Nevertheless, reactive and active power is varied if there are disturbances or nonlinear loads connected across a generator or a set of generators in a power system. Nonlinear loads are becoming more popular in power systems, especially in distribution systems, where the structure of most electrical apparatuses contains power electronic devices (P Bapaiah, 2013). Since electronic power loads have a wide separation compared with conventional loads due to the development of devices that work based on the electronic switches in their structure, such as welding plants, factories of cars using automation (robots), advanced hospitals, Cycloconverter, etc. Since the operation of these loads is depending on the switching process of the switches, it causes contamination of the power system and causes a reduction in the Power Quality (PQ). This decrease in PQ has a bad effect on the power system, where it causes a variety of system stability to increase in losses and reduce efficiency. Therefore, it is important to improve PQ. Different approaches are used in this field to enhance the PQ of power systems such as Static Var Compensator (SVC) and Static Synchronous Compensator (STATCOM) have been used to inject a reactive power in the system to improve the power quality by reducing the Total Harmonic Distortion (THD%) and power factor correction. In the last or since the appearance of STATCOM was taken reactive power compensation from the source. The capacitor in the STATCOM is responsible for generating reactive power, and where the charge of the capacitor is taken from the source via the voltage source converter for STATCOM. This power from STATCOM is injected a second time into the system, this case causes the power consumed to add from the main source. And some of the studies used Photovoltaic (PV) panels to feed the voltage source converter for STATCOM (Georgios and Georgios, 2011). Where they can inject the active and reactive power from PV panels, but remain this way insufficient because of variable radiation and temperature of solar in the day, month, and year.

Some of the other studies resolved the problem of solar energy by replacing the PV panels with the batteries. Furthermore, here the batteries fed the VSC for STATCOM to produce active and reactive power compensation. But also, the batteries needed after discharge to charge in addition to the problem of the deep cycle has in the batteries where each battery have a deep cycle different from others (Arindam, et al., 2012).

The compensation mechanism can be divided into two parts, the first is a static synchronous transmission line compensator called STATCOM for the transmission line, and the second is a static synchronous distribution compensator called DSTATCOM (Marcelo, 2008; Irena, 2008).

Due to the widespread renewable energy sources, many researchers focused their works on introducing it as an input to the STATCOM device, which has been used to enhance the power quality of distribution systems. To ensure broadening the use of non-linear and linear electrical loads, and to solve the transmission and distribution problems. Therefore, renewable energy has become the best choice concerning fossil fuel, which causes environmental pollution in addition to high exploration and extraction prices (Mukhtiar, et al., 2011).

Solar energy has many advantages over other types of sources, the first important one is sustainability, free energy, and also environmentally friendly. Increasing the solar power output is relating to the increase of solar radiation and the effects of the temperature (Maan, et al., 2018). Thus, if the amount of solar radiation increases during the day, power production increases. While the temperature rise above the limits rates of the solar panels leads to a decrease in the generated power in the solar panels. Therefore, it is necessary to take into consideration the effect of temperature change, amount of solar radiation through the daytime. In Iraq and some governorates, the mean intensity of solar radiation and temperatures were measured (Fayadh and Yarab, 2014).

The storage energy unit (batteries) is considered an important factor for storing surplus energy when it is connected to solar panels. Batteries normally are used to store the excess power and supply it during the night and on cloudy days. Lead-acid batteries have been considered the most popular used, as it has acceptable specifications, an average good life, and an affordable price (Igor, 2006). Also, the

values of solar radiation and the temperature of solar can be represented in the simulation by repeater block or constant block. Besides, the illumination of the sun and the temperature can be measured realistically by the Arduino Mega 2560 (Siti and Mohamad, 2018).

For many reasons, hybrid systems that are applied with renewable sources such as solar energy, wind turbines, and batteries have become the focus of the attention of researchers in the areas of the use of ordinary inverters. All this due to include flexibility in supply, which leads to maintaining the stability of loads without interruption and reduction of fuel cost. In addition to decreasing emissions of gasses that pose danger on the people and environment. Most previous works used renewable energy systems as separate from the STATCOM or they used STATCOM with one source on the dc-link of VSC for STATCOM like PV or batteries (Rajiv, 2018; Zhiping, 2001). But in this thesis, the STATCOM is based on photovoltaic array and batteries as a hybrid source system to compensates both active and reactive power at the same time (Firas, et al., 2020).

The photovoltaic array generates a DC power which has a variable magnitude because it depends on the sun radiation falling on the panel and the temperature. Therefore, it is necessary to regulate this DC power by DC-DC boost converter circuit (Ramon, et al., 2018). The circuit has been used to supply the three legs of the VSC with constant voltage (Shih-Kuen, 2010). The generated pulses of Isolated Gate Bipolar Transistor (IGBT) is known Pulse Width Modulation (PWM). This method has a high switching loss because it did not predict the value of variable input voltage generation from photovoltaic cells (PV). A Maximum Power Point Tracking (MPPT) algorithm has been used to track the Maximum Power (MP) between an input voltage (Vpv) and current (Ipv) find the Maximum Power Point (MPP) between them (Laguado-Serrano, et al., 2019).

The MPPT algorithm is used to make maximum use of the power generated by solar panels (Deepak et al., 2015). The MPPT algorithm can be represented in many ways like the Constant Voltage method (CV), the Open Circuit Voltage method (OCV), Short Circuit Current method (SCC), the Perturb and Observe method (P&O), modified P&O, and Incremental Conductance method (INC), etc (Pallavee and RK, 2013). The Incremental Conductance method (INC) is considered

a good method used to find a suitable Duty cycle (D) of the IGBT switch for boost circuit (Safari and Mekhilef, 2011).

The contribution of this work has been represented by connection sources PV and batteries as a source for a three-leg of Voltage Source Converter (VSC) for Distribution STATCOM (DSTATCOM). When the generated power of the solar panels is increased more than the system power demand, the increased power has been used for battery charging. Also, it is important to regulate the batteries charging power when the PV panels generates high energy. During the night or cloudy days where the generated power of PV panels is low, the batteries is used to supply the load requirements from the stored energy during the day. Also, a DC to DC buck-boost circuit has been introduced to control the charge and discharge intervals of the batteries (Avjs and Sheldon, 2019). Since the PV panels generate high power through and supply the necessary power to the inverter, the buck converter was used to store the additional generated power in the batteries. The boost converter has been used to supply the load demand during the night or cloudy days. A high coordination between solar panels and batteries are essential to improve the performance of the hybrid system (Sarina and Fangxing, 2014).

The main goal of any compensation system is to have a flexible and fast response to power system performances. In general, the control circuits of STATCOM have depended on voltage and current measurement in the location in which disturbance happens, to compute the amount of increase or decrease in the voltage or current through special equipment which works on the measure the difference between the location of the disturbance and the set values of design of compensation equipment STATCOM (Majid and Mansour, 2014). Furthermore, the methods of representing the control circuit of compensation equipment STATCOM is very important to process required compensation. Many methods had been used to represent the control circuits for STATCOM such as, phase shift control method, decoupled current or direct and quadrature (d-q) control method, Synchronous Reference Frame Method (SRFM), Instant Symmetrical Part theory (ISPT) and Synchronous Reference Frame Method with Unit Vector (SRFMUV) (Metin, 2011; Reyes, 2009; Amit, 2018). Every one of these methods is used according to the type of applied load, type of power grid, and the amount of required compensation. It has

been noted that SRFM and SRFMUV are usually used to compensate for a three-phase current source with a non-linear load, decoupled current method (d-q) is used to increase the generated compensation active and reactive power (Tabatabaei, et al., 2015).

But it required continuous modification of its parameters to keep the compensation with the required level. Also, it has some drawbacks where it delays the compensation process with a reduction in its time response. After selecting one of the above methods, an appropriate compensation angle is adopted based on different control approaches to switch the insulated-gate bipolar transistor (IGBT) or Gate Turn Off thyristor (GTO) pulses within the voltage source converter (VSC) circuit (Naeem, et al., 2009).

The IGBT is ideal for use in power electronics applications, and a semiconductor switching system. The main benefit of the IGBT is a greater gain compared to BJT combined with higher voltage output and lower input losses in transistors such as the MOSFET. The voltage blocking capability of faster devices such as IGBT and the switching speed of GTO thyristor high voltage devices is normally found to be limited (Widjaja et al 1995). If the high power is needed for compensation, we will choose GTO in the switch, while if we have limit for power (low power compensation) chosen the IGBT in the switch (Rajiv and Reza , 2017).

In this thesis, two types of power sources PV system (Solar panels and Batteries) have connected across the DC link of the DSTATCOM device to enhance the performance and increase the time response of the grid. A Synchronous Reference Frame with the Unit Vector Method (SRFUVM) is used to control the operation of the DSTATCOM (Jou, et al., 2008).

The generated power of solar panels is dependent on the radiation of solar and the temperature of the solar. Therefore, it has been represented in MatLab Simulink by a block known as (a repeating table) block this table can represent variable radiation and temperature according to the use day time. Also, the MatLab Simulink environment enabled a new hardware support package for the 2017-2019 versions to work with the Arduino interface. So, this feature took advantage of a true measure of solar radiation and the degree of heat through the Arduino as entries for Simulink to make the representation of the system closer to reality (Agbetuyi, et., al 2018).

CHAPTER ONE

LITERATURE REVIEW AND THESİS LAYOUT

1.1 Literature Review

(Mercado, et al, 2006), discussed the performance of a batteries connected across the DC link of multi-level voltage source converter (VSC) of DSTATCOM, the Synchronous reference frame was used to represent the control circuit for DSTATCOM. The results are obtained without batteries fed the DC-link DSTATCOM (alone). And with a battery connected on the terminals of DSTATCOM DC-link. When the batteries are used to feed the DC-link of VSC for DSTATCOM has gated compensating active and reactive power and reduced total harmonic distortion (THD%) of current source inverter. The drawback of the work is that it can't be applied practically, where the batteries can't be connected without a charging source to maintain the minimum allowable of storage level of the batteries, in addition to limited batteries life limited (deep cycle).

(V. Kamatchi and N. Rengarajan, 2012) Presented a three-phase four-wire distribution static compensator (DSTATCOM). A DC-DC boost converter three-leg DC link of DSTATCOM supply from photovoltaic panels (PV) or batteries, and a star-delta transformer has connected between DSTATCOM and the non-linear load. A Synchronous Reference Frame Theory (SRF) has used as a control technique for the DSTATCOM. It has been applied to maintain supply the load with reactive power and improve the total harmonic distortion (THD%). The THD% of the three-phase current source equal to 27.28% and 5.4% before and after compensation respectively. A Star-delta transformer was applied to a balance of load by close cycle current in delta connects. A renewable energy source (PV panels) was connected across the DC link of the DSTATCOM to ensure the supply of the required level of active and reactive power.

(V. Kamatchi and N. Rengarajan, 2014) Proposed a three-phase three-wire with DSTATCOM fed by a PV-batteries supplied by DC-DC boost converter circuit is proposed. Where the DSTATCOM was used to enhance the power quality of the distribution system. A star-delta transformer was connected between DSTATCOM and non-linear load. A star-delta transformer was worked to balance of three-phase

load when the load becomes unbalanced. The reactive current approach has introduced in the control circuit algorithm of the DSTATCOM. Also the fuzzy logic control has used for tuning the PI controller of the voltage regulator. DSTATCOM was used to reduce the harmonic components of the current source, and reactive current compensation with comparing the results in case of using the fuzzy PI controller tuning and without using the fuzzy PI controller. The researcher did not use the (PV or batteries) with DSTATCOM to compensate for active power, but just uses the ANTFS of the PI controllers in the control circuit of DSTATCOM.

(Digvijay, et al, 2015) Suggested DSTATCOM device to be connected with a three-phase four-wire with unbalancing the load and non-linear load. A DC-DC boost converter set up the output of PV panels or batteries to match the STATCOM DC link voltage. The insulated-gate bipolar transistor (IGBT) switch is used for the three-legs of VSC. An SRF theory is used as a control circuit of DSTATCOM. The Unbalance load was balanced by the Star-Delta transformer. DSTATCOM is used for power quality improvement, to compensate for the reactive and active power and power factor correction.

(Shaik, et al, 2016) Presented power quality issues like voltage waveform distortion, voltage sag and swell, increase reactive power, THD and power factor which has a great effect on dynamic characteristics of the power grid system. Different methods are used to mitigate their effect on the system parameters to enhance stability and PQ issues. DSTATCOM based on the Batteries Energy Storage System (BESS) across the DC link capacitor of the voltage of three-leg connected to the Point of Common Coupling (PCC) has adopted in this work. DSTATCOM and wind generators are feed linear and non-linear loads at the same time. Usually, the output power of the wind generator is unstable, therefore the BESS device is connected across the DC-link to suppress problems caused by changes in wind power. The unit vector method has been used for the control circuit of DSTATCOM. It is found that the power quality issue can be improved and the total harmonic reduced (THD) by injecting a current source of VSC in the grid.

(Om and Abdu, 2016) Suggested a power quality improvement issue due to faults occurring like trip and reclose of feeder load flickering, voltage sag, and swell. In addition to the PQ related to problems of wind energy systems like outage and

synchronizing with in addition to the variation of wind speed has considered. The DSTATCOM was connected with DC-link capacitor voltage to obtain active and reactive power compensation. Also, to regulate voltage, frequency, and minimize the total harmonic distortion (THD). An SRF theory is considered as a control circuit of DSTATCOM, a modified IEEE 13 node with a wind generator was applied in the case study. The BESS system with DSTATCOM suppresses problems caused by variations in wind generator power due to climate change in the wind. The results showed that the DSTATCOM based on SRF can effectively improve the PQ of the distribution system with wind turbines during the disturbance of the power system and enhance the THD which has been reduced by less than 5%.

(Amit et al., 2019) The authors suggested a batteries energy storage system (BESS) across the dc-link capacitor with distribution synchronous compensator (DSTATCOM) system (DSTATCOM) to improve overall power quality Different PQ issues were considered in the paper which involve, reduction of total harmonic distortion, power factor correction, etc. Three strategies have been used in the control circuit for DSTATCOM Synchronous Reference Frame (SRF), Instantaneous Reactive Power (IRP), and Power Balance Theory (PBT). The type of maximum power point tracking (MPPT) has been used to Perturb and Observed (P, O) of active and reactive power due to outage or synchronization of the generator or the tripping the non-linear load. The results have shown the high performance of PBT compared with the different control methods applied in this work. A comparison also was performed when the conventional DC-link capacitance without PV panels as an input across the DC link of the DSTATCOM device. Also, the results in this point show a high performance of PBT and the lowest performance recorded in the IRP.

(Kavita et al., 2019) for power quality improvement. Supposed a method to optimize the dc-link of three-legs voltage source converter (VSC) for DSTATCOM. A Reduced Switch Count Multi-Level Converter (RSC-MLC) with photovoltaic PV panels connected has a feed in the control circuit of DSTATCOM to compensate both active and reactive power, reduced the total harmonic distortion (THD), and power factor correction. It can supply real power as a support to the load which avoids overloading the source. The DC link voltage can be controlled based on RSC-MLC, where it reduces the DC link to a minimum value when the load in off-peak

and increase its value during full load. This can reduce the stress on the power electronic switches in addition to reduce switching losses. The voltage of PV array has boosted to the DC link value using in boost converter and connected across the RSC-MLC. Perturbation and Observation (P&O) have been used to obtain the maximum power point tracking of the PV arrays. The results have shown a good performance of the suggested strategies (RSC MLC) and THD of the current source within limits of the standard of IEEE 519 [40]. The references closest to the works using in this thesis are the source [25], where it has been applied the same parameters in terms of the case study and the non-linear load and star/delta transformer in the model.1a. Reference [37] the same idea used in the model.1b in terms of power quality improvement for renewable using DSTATCOM. The same parameters of the case study and the case test in the model.2 have been applied in reference.

1.2 Aims of the Work

i. Provide simultaneous coordinated design between multi-sources Photovoltaic panels (PV system) across the dc-link of Voltage Source Converter (VSC) of the STATCOM in three ways.
ii. The real-time signal taken from the Arduino sensor as represented (irradiation and temperature) is connected in Matlab 2018a Simulink, signals are fed in the dc link for STATCOM.
iii. By improve the power quality of the source via reducing the total harmonics distortion (THD%) for the three-phase current source.

1.3 Thesis Layout

The work in this thesis is organized within five chapters and as follows:

Chapter 1 includes ***"Introduction and Literature Review"***, aims study and organization of thesis to use PV system with STATCOM to solve power quality problems.

Chapter 2 In this chapter, The theoretical basis of the control circuits models Synchronous Reference Frame Method with Unit Vector (SRFWUV). The voltage sources converters reviewed (types and their applications). Mathematical model of Photovoltaic cell, the mathematical analysis of boost converter circuit of (PV panels)

are analyzed. The method of control on the switch in (PV panels) boost circuit by Maximum power point tracking (MPPT) using Incremental Conductance method (INC) has been introduced. The mathematical analysis of bi-directional DC-DC Converters for energy storage.

Chapter 3: In this chapter, the complete systems Design and simulation of model. The design include DSTATCOM is fed from PV system (PV panels and batteries).

Chapter 4: In this chapter, analysis and discussion of the simulation results, the design work has been applied for three cases, STATCOM without PV system with Non-linear load, STATCOM with PV system with Non-linear load (variable irradiation and temperature), and STATCOM with PV system (real time signal from Arduino sensors).

Chapter 5: "Conclusions and Suggestions for Future Work" finally, this chapter thoroughly discusses the established conclusions and future work suggestions.

CHAPTER TWO
THEORETICAL AND BACKGROUND OF STATCOM

2.1 Introduction

Power compensation is considered as an important issue during evaluating the dynamic performance of the electric grid under different operating conditions. Therefore, it is important to study the structure of static synchronous compensator (STATCOM) and the equivalent circuit of it. Also, it is useful to analyze the performance of the compensation for STATCOM, so it was studied the performance of compensation at ignored the electrical transient losses in the AC and DC power circuits of the STATCOM. And also, is selecting the converter's square wave switch operation and ignoring the harmonics that produced on the load, so the analysis becomes more simplistic. Generally, STATCOM is used to maintain the stability of both transmission and distribution power systems, improve voltage regulation, power factor correction reduces load fluctuations or imbalance, and decrease (THD%) (Digvijay, et al., 2015).

There are several control methods that had been used to simulates the control circuit of STATCOM. In this work, a detailed explanation of the most common control methods to regulate the active and reactive power compensation. In this work a Synchronous Reference Frame (SRF) with Unit Vector (UV) and decoupled current control (d-q) theory has been considered as a control approach to regulate active and reactive power compensation of DSTATCOM. The SRF with UV is described in detail with an additional explanation of the PV panels boost, a buck-boost of the batteries, and high coordination between circuit with voltage source converter (VSC). A conventional PI controller has been usually used with these systems to control DSTATCOM's compensation due to low cost, user-friendly, and simple to construct. In the first work, two PI controllers have been used with the control circuit of DSTATCOM. The PI controllers of dc and ac voltage regulators have been used in the first circuit where the try and error training method is applied to regulate the PI parameter gains.

2.2 STATCOM performance with input Sources PV system

STATCOM with input Sources PV system (PV and battery) has been considered avoiding voltage variability and active and reactive power control of

three-phase for a voltage of the system. The voltage and frequency of the grid are varied continuously due to variation of applied load, permanent and transient faults, and rapid increase or decrease of the power demand. Therefore, it is important to provide suitable compensation for the effects of these disturbances that occur in the distribution power systems. STATCOM is an important device that had supplied both active and reactive powers to improve the performance of the electric grid. The PV system (PV panels and Battery) source have been suggested in the current thesis to supply the required active power for compensation from a renewable energy source, which is connected across the DC link for the capacitor as shown in "Figure (1)".

The hybrid voltage source for inverter normal has been used in this thesis, with the same parameters in renewable energy that has been used to feed the DC link for STATCOM. While the control circuit of STATCOM fed on the multi-power sources (PV panels and batteries) is designed to control the amount of compensated active and reactive powers according to variation of the grid operating conditions. Also, it is used to absorb the active and reactive power if the system voltage is swelled.

"Figure (1)" shows the simple structure of the methodology for this thesis if the Voltage-STATCOM (VSTATCOM) output voltage is in line with the terminal Voltage of the bus (Vbus) and VSTATCOM is higher than Vbus of the STATCOM, then it supplies the system with active and reactive power. If the voltage of STATCOM is smaller than Vbus, STATCOM absorbs active and reactive power from a power system. If STATCOM and Vbus are equal, then, in this case, no compensate or absorbed power is applied to the system, where the STATCOM operates in floating mode (Parimal, et al., 2014).

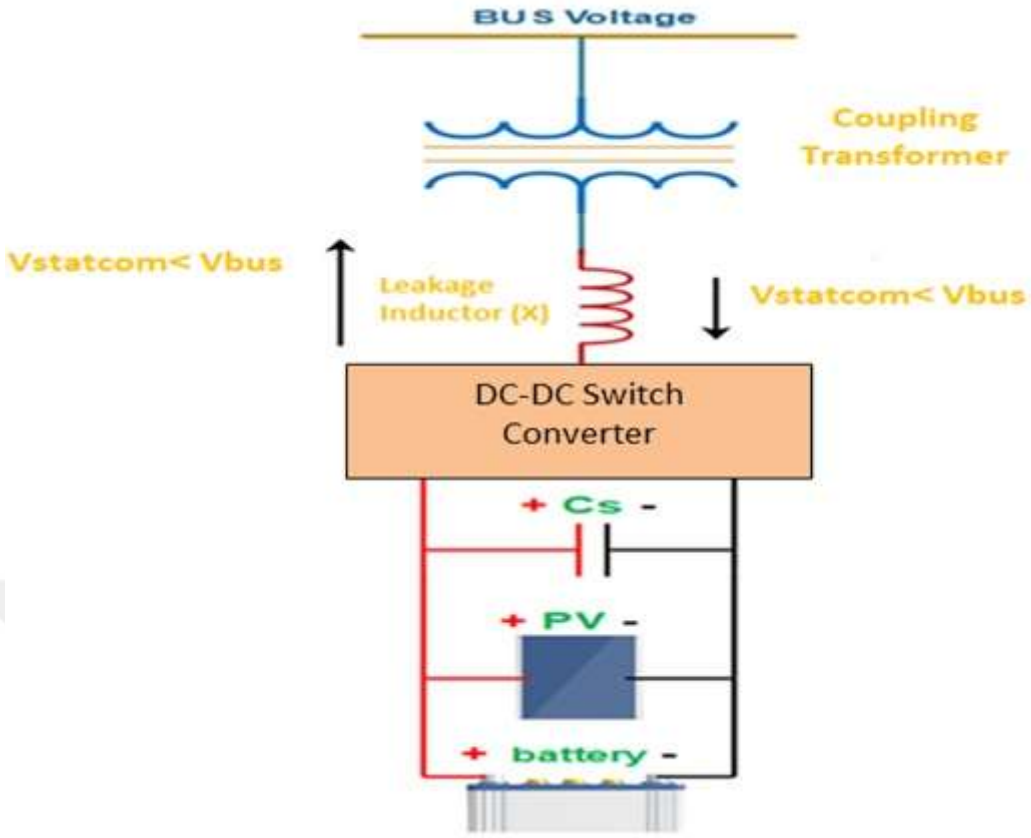

Figure 1. Schematic diagram of STATCOM with multi-power sources PV system.

2.3 Mathematical of STATCOM

The general equations of STATCOM used to represent the generated active and reactive power can be expressed in the equations (2.1) and (2.2) respectively (Parimal, et al., 2014):

$$P = \left(\frac{V_{Bus}\, V_{statcom}}{X_L}\right) \sin\alpha \qquad (2.1)$$

The basic equation of reactive power compensation of STATCOM can be computed from:

$$Q = \left(V_{Bus}\, \frac{V_{Bus}}{X_L}\right) - \left(\frac{V_{Bus}\, V_{statcom}}{X_L}\right) \cos\alpha \qquad (2.2)$$

Where: (P and Q) are generation or absorption the active power and reactive power from grid or STATCOM respectively, and X_L is the impedance of coupled transformer. STATCOM is similar in principle but differs in terms of the purpose of use in compensation. Different control strategies are used to construct the control circuit of STATCOM which can be listed below:

i. Phase Shift control theory (Metin, et al., 2011).

ii. Decoupled Current control (d-q) Theory.

iii. Synchronous Reference Frame theory (Reyes, et al 2009).

iv. Instant Symmetrical Part Theory (Amit, et al 2018).

v. Synchronous Reference Frame with Unit Vector theory.

In the this work, two types of control approaches have been used. The first control method is the SRF with a unit vector (UV) ((Widjaja et al 1995), and the second control method decoupled current (d-q) (Tabatabaei, et al., 2015). The three-phase AC components are transferred into DC type based on the $(d-q)$ reference frame axis. Control techniques on DC components are simple and easy to apply compared with control methods that apply to the three-phase AC components which vary in nature with time (Amirnaser, 2010).

2.3.1 Transformation from (abc) to $(d-q)$ axis

Three-phase electrical components, such as voltage, currents and powers could be represented by a transporter known as stationary reference frame (Schauder and Mehta, 1993). The vector depiction of the instant three-phase variables in the abc stationary reference frame is shown in "Figure (2)"

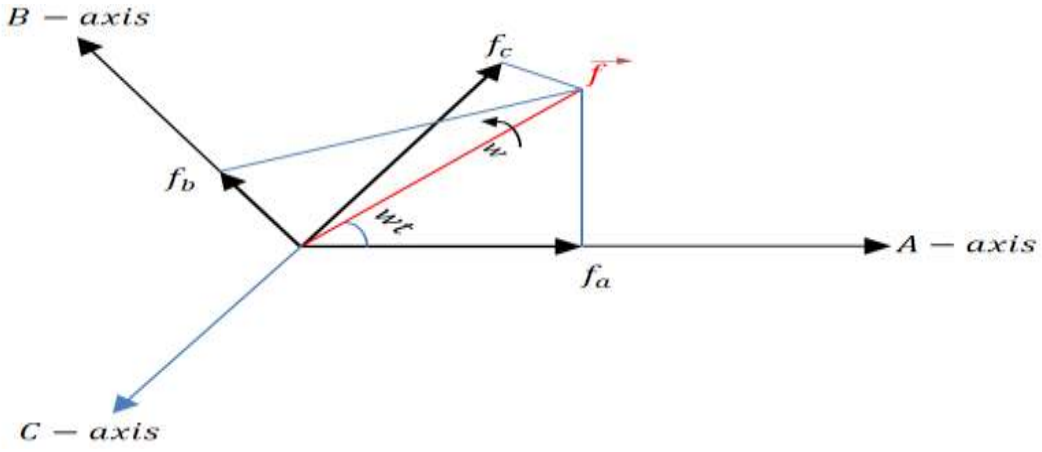

Figure 2. Phaser diagram of Vector depiction in three-phase [44].

The vector (f) is calculated by [44]:

$$f(t) = \frac{2}{3}\left(fa(t) + fb(t)e^{j\frac{2\pi}{3}} + fc(t)e^{-j\frac{2\pi}{3}}\right) \quad (2.3)$$

Where $fa(t)$, $fb(t)$ and $fc(t)$ are calculated in equations:

$$fa(t) = M\cos(wt) \tag{2.4}$$

$$fb(t) = M\cos\left(wt - \frac{2\pi}{3}\right) \tag{2.5}$$

$$fc(t) = M\cos\left(wt - \frac{4\pi}{3}\right) \tag{2.6}$$

Where: (M) is the magnitude in each electrical phase vector and (w) is the synchronous rotational angle (377 rad/sec) of the vector, (wt) is the synchronous rotational angle change with time. In a rotated reference, the frame consists of direct and quadrature axis (d − q), such three-phase variables can be transfigured into two-phases variables within synchronous reference frame. The transformation is performed as follows (Paul, et al., 2013).

$$\begin{bmatrix} f_d \\ f_q \\ f_o \end{bmatrix} = \frac{2}{3}\begin{bmatrix} \cos(wt) & \cos(wt - \frac{2\pi}{3}) & \cos(wt + \frac{2\pi}{3}) \\ \sin(wt) & \sin(wt - \frac{2\pi}{3}) & \sin(wt + \frac{2\pi}{3}) \\ \frac{1}{2} & \frac{1}{2} & \frac{1}{2} \end{bmatrix}\begin{bmatrix} fa \\ fb \\ fc \end{bmatrix} \tag{2.7}$$

The phaser diagram has obtained the transformation from (a, b, and c) to the direct and the quadrature axis represented in the "figure (3)". Here, (fd and fq) are the vector components in d − q axis.

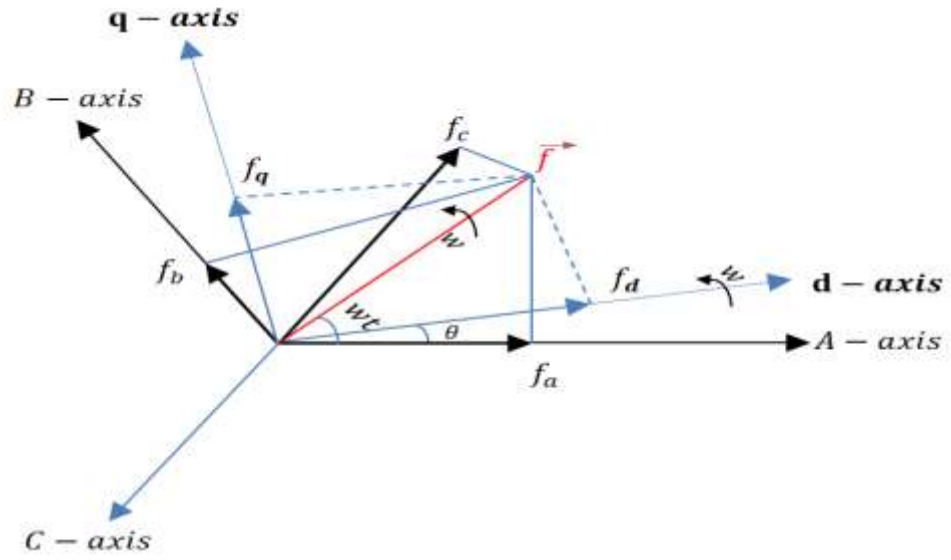

Figure 3. The phaser diagram of the (d − q) reference frame.

Both fd and fq components are obtained from this transformation, where the vector f(t) can be calculated by equation (2.8).

$$f(t) = (fd + jfq)e\,j\omega t \quad (2.8)$$

2.4 The Mathematical design of control circuit for DSTATCOM

As it is sated previously, two types of control approaches have been considered, to control the operation of the DSTATCOM, a Synchronous Reference Frame Method with Unit Vector (SRFMUV) is considered in this chapter. The schematic diagram of SRFMUV as illustrated in "Figure (4)".

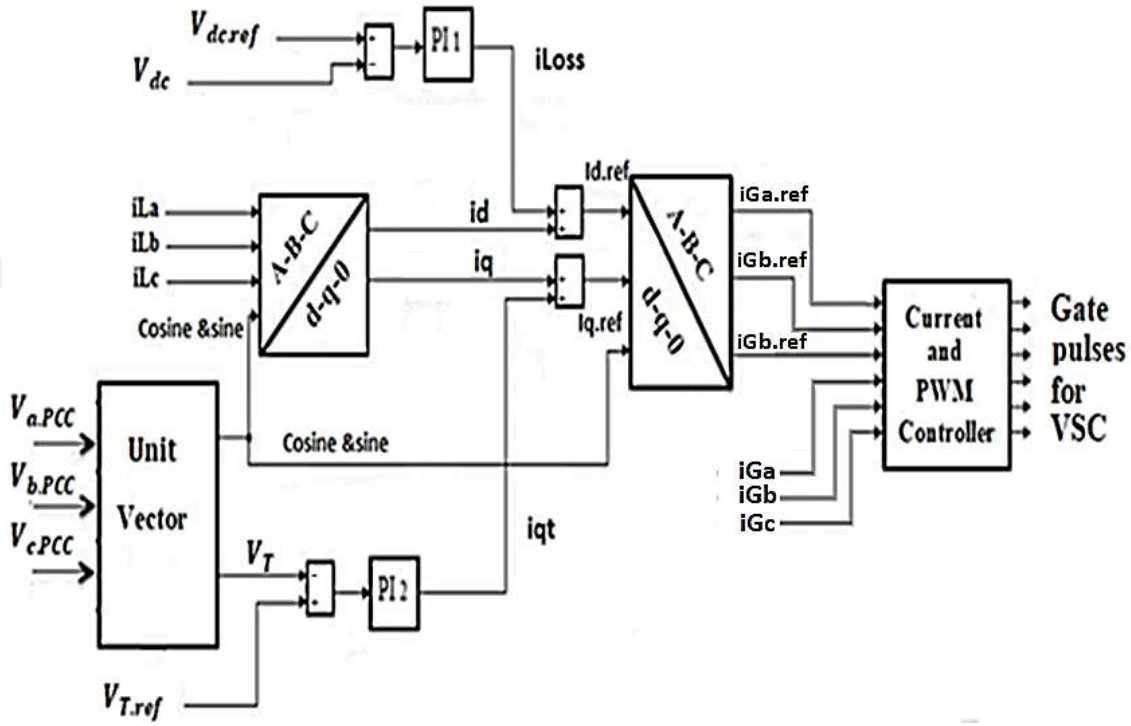

Figure 4. Schematic diagram of SRFMUV control approach.

The mathematical equation is represented as follow (V. Kamatchi and N. Rengarajan, 2012):

In equation (2.9) the currents (id, iq), has been computed in $(d-q)$ axis.

$$\begin{bmatrix} i_d \\ i_q \\ i_o \end{bmatrix} = \frac{2}{3}\begin{bmatrix} \sin\theta & \sin(\theta-\frac{2\pi}{3}) & \sin(\theta+\frac{2\pi}{3}) \\ \cos\theta & \cos(\theta-\frac{2\pi}{3}) & \cos(\theta+\frac{2\pi}{3}) \\ \frac{1}{2} & \frac{1}{2} & \frac{1}{2} \end{bmatrix}\begin{bmatrix} ila \\ ilb \\ ilc \end{bmatrix} \quad (2.9)$$

The Unit Vector method is expressed in "Figure (5)", and the magnitude is evaluated using equations (2.10) and (2.11).

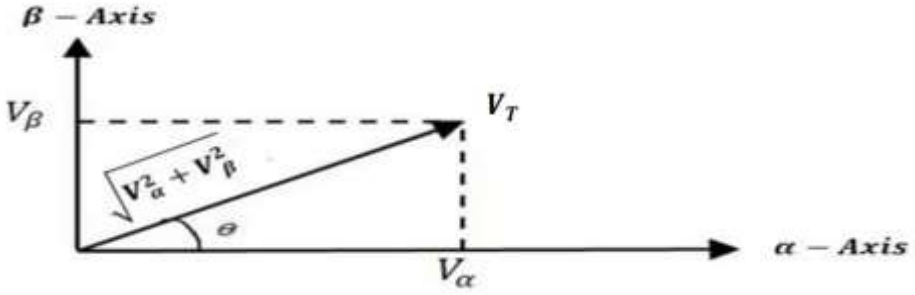

Figure 5. Pharos diagram of Unit Vector method.

The three-phase voltage (abc) is converted into stationary *reference* frame αβ0 which is computed by:

$$\begin{bmatrix} V_\alpha \\ V_\beta \end{bmatrix} = \begin{bmatrix} 1 & -\frac{1}{2} & -\frac{1}{2} \\ 0 & \frac{\sqrt{3}}{2} & -\frac{\sqrt{3}}{2} \end{bmatrix} \begin{bmatrix} V_a \\ V_b \\ V_c \end{bmatrix} \quad (2.10)$$

$$V_T = \sqrt{V_\alpha^2 + V_\beta^2} \quad (2.11)$$

(V_T) is the magnitude of vector voltage in the $(\alpha - \beta)$ stationary reference frame. And $\cos\theta$ and $\sin\theta$ can be computed by equation (2.12) and (2.13).

$$\cos\theta = \frac{V_\alpha}{V_T} \quad (2.12)$$

$$\sin\theta = \frac{V_\beta}{V_T} \quad (2.13)$$

The current loss of dc and represented the out signal of PI controller.1. It has been used for compensation from the losses of IGBT switch converter for DSTATCOM, which can be calculated in equation (2.14).

$$ilos(k) = ilos_{(k-1)} + K_{pdd}\left(V_{dcE(k)} - V_{dcE(k-1)}\right) + K_{idd}V_{dcE(k)} \quad (2.14)$$

Where: $(ilos(k)$ and $ilos(k-1))$ are the loss current in $d-$ axis at the (k) sample of the waveform current and the current loss in $d-$ axis when the k sample subtracted from 1 respectively, $\left(V_{dcE(k)}\right.$ and $\left.V_{dcE(k-1)}\right)$ are the dc voltage applied at the k sample within the PI controller.1 and the dc voltage at k subtracted from 1 respectively, and the $(K_{pdd}$ and $K_{idd})$ are the proportional gain and integral gain of PI controller.1 respectively.

The $(i_{d.ref})$ has represented reference current in $d-$ axis in arbitrary reference frame, given by equation (2.15).

$$i_{d.ref} = i_d + i_{loss} \quad (2.15)$$

Where: (i_d and i_{loss}) are the current in the $d-$axis and add to the amount of current loss that computed in equation (2.14) respectively.

The $i_q(k)$ represented the output signal of PI controller.2 in $q-$axis in reference frame as explain in equation (2.16).

$$i_q(k) = i_q(k-1) + K_{pq}\left(V_{T(k)} - V_{T(k-1)}\right) + K_{iqt}\, V_{T(k)} \quad (2.16)$$

Where: ($i_q(k)$ and $i_q(k-1)$) are the current in $q-$axis at (k) sample and the current in q-axis when (k) sample subtracted from 1 within the PI controller.2 respectively, $\left(V_{T(k)}\right.$ and $\left.V_{T(k-1)}\right)$ are the magnitude of vector voltage (V_T) in the PI controller.2 at (k) sample and the magnitude of vector voltage when the (k) sample subtracted from 1 within the PI controller.2 respectively, and (K_{pq} and K_{iqt}) are the proportional gain and integral gain of PI controller.2 respectively.

Now the quadrature current reference ($i_{q.ref}$) is calculated from equation (2.17).

$$i_{q.ref} = i_{qt} + i_q \quad (2.17)$$

Through the equations (2.15) and (2.17) can be calculate the current (i_α) and (i_β) are the current in stationary reference frame in equations (2.18) and (2.19).

$$i_\alpha = i_{d.ref}\sin\theta + i_{q.ref}\cos\theta \quad (2.18)$$

$$i_\beta = i_{d.ref}\cos\theta - i_{q.ref}\sin\theta \quad (2.19)$$

The current in $d-q$ reference frame to three-phase current (abc) is considered reference current signal are computed by the matrix (2.20).

$$\begin{bmatrix} IGa.ref \\ IGb.ref \\ IGc.ref \end{bmatrix} = \begin{bmatrix} 1 & 0 \\ \frac{-1}{2} & \frac{\sqrt{3}}{2} \\ \frac{-1}{2} & \frac{-\sqrt{3}}{2} \end{bmatrix} \begin{bmatrix} I_\alpha \\ I_\beta \end{bmatrix} \quad (2.20)$$

After calculating reference currents of equation (2.20), it was compared with currents of the generator affected by the disturbance or nonlinear load. Then based on the PWM technique suitable pulses, are generated for triggering DSTATCOM using IGBT switches.

2.5 Voltage Source Converter

The principle of transforming DC to AC, voltage inverter, or converters, in general, is groups of switches connected in a manner to provide chopping for a DC source and inverted in shape close to an AC waveform. But this ac waveform contains on a distortion because the losses of switch converters and a high harmonics of dc voltage converters, to calculate the harmonic distortion by (Chung and Hsin, 2014):

$$\text{THD} = \frac{\sqrt{I_s^2 - I_{s1}^2}}{I_{s1}} 100\% \qquad (2.21)$$

Where: I_s and I_{s1} are the rms value of current converter and fundamental current of the converter respectively.

There are two main types of converters of the STATCOM:

1- Voltage Source Converter (VSC).

2- Current Source Converter (CSC).

The voltage source converter which is commonly used more than the current source converter due to (Braz, et al., 1997):

i. Current source converters need bi-directional voltage-blocking control electronic components. The obtainable heavy-power semiconductors to GTOs (IGBTs) are unable to block reverse voltage any more or must do so with such a detrimental effect on other essential variables.

ii. The use of a voltage-charged capacitor to insert the converter is preferable on the use of a current-charged reactor because the induction causes a greater energy loss.

iii. The current-sourced converter needs termination of the voltage source near ac terminals, typically on the form of the capacitive filter, as shown in "Figure (6)"

iv. Because there is a large DC capacitor in the input of VSC, it protects semiconductor switches GTO and IGBT, as illustrated in "figure (7)".

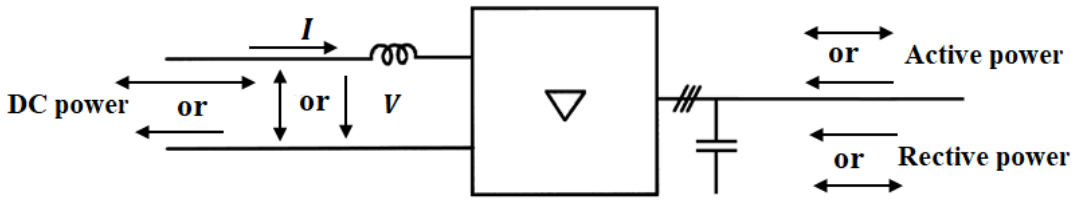

Figure 6. Basic principles of Current Source Converter (CSC) (Bina, and DC, 2005).

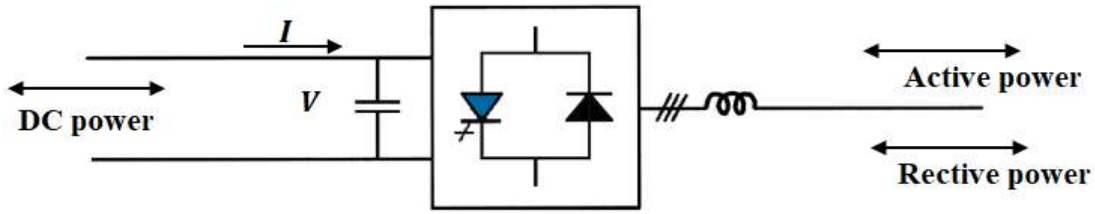

Figure 7. Basic principles of Voltage Source Converter (VSC) (Bina, and DC, 2005).

The converters of STATCOM is the three-phase output voltage produced by a voltage-sourced DC to AC transformed operated from an energy storage capacitor to generate suitable compensation. And the types of converters most commonly used like (Juan, et al., 2005).

2.6 Solar Energy

There are several types of renewable sources, like solar energy, wind energy, and tide energy, etc (Jan, 2008; Askari, 2015). In the current thesis, solar energy has been used which is consider one of the most important energies used over the world and especially in Iraq, where to consider Iraq is one of the countries rich in solar energy (Igor, 2006). This energy needed to collect the radiation of solar by crystal cells known as a photovoltaic cell. There are three basic types of solar cells, such as monocrystalline solar cells, polycrystalline solar cells, and thin-film solar (Kirubakaran Victor and Muthu, 2014).

In the thesis, the type of solar cell has been used (the heterojunction with intrinsic thin layer) solar cell made of a thin monocrystalline silicon wafer surrounded by ultra-thin amorphous silicon layers. This product provides the industry‘s leading performance and value using state of the art manufacturing techniques (Kazem and Meysam, 2019).

The type of output power from the solar panels is variable dc-power. Therefore, it used the boost converter circuit to regulate the output of dc power for it (Laguado-Serrano, et al., 2019).

2.6.1 The Mathematical Model photovoltaic (PV) cell

The PV cells farm consists of numerous modules (panels) connected in parallel and series mode to provide the required current and voltage for the design. In figure (8), the equivalent electrical circuit of the photovoltaic module PV

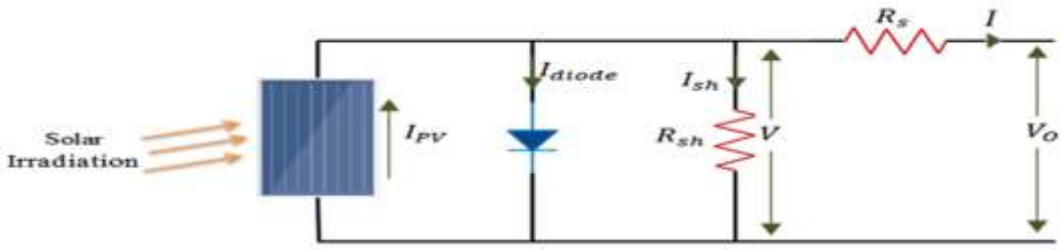

Figure 8. Equivalent electrical circuit of photovoltaic Module PV(V Kamatchi and N Rengarajan,2012).

The variation of solar radiation is mathematically described by a following equations (Sarina and Fangxing, 2014):

$$I = I_{PV} - I_{sat}\left[\exp\left(\frac{Vo\ Qe}{N_c B T_d\ i}\right) - 1\right] - \frac{V_o}{R_{sh}} \quad (2.22)$$

$$V_o = V + R_S I \quad (2.23)$$

The current of PV panel is based primarily on the two variables, first is the linearity of solar radiation, second is the temperature of a PV cell as indicated in the equation (2.24).

$$I_{PV} = \left(I_{PV,s} + K_t\ \Delta t\right)\frac{G}{G_n} \quad (2.24)$$

The value of $I_{PV,s}$ can be calculated from the equation (2.25) that represented the equivalent electrical circuit of "Figure (10)" (Sarina and Fangxing, 2014).

$$I_{PV,s} = \frac{R_{sh} + R_s}{R_{sh}}\ I_{sh} \quad (2.25)$$

Where: (I_{PV}) and (I_{sat}) are the photo diode and saturation currents respectively, (N_c) is the number of cells that are connected in series, (B) is the boltzmann constant, (T_d) is the diode temperature of $p-n$ junction, (Qe) is the elctronic charge, (R_{Sh}) repersents the shunt resistance of the equivalent electrical circuit array, (R_S) repersented the series resistance of equivalent electrical circuit array, (i) is the ideality factor and lies within the range $1 \leq i \leq 1.5$ and choosed 1 in this thesis, $(I_{PV,s})$ is the photo current condition of (STC, 25℃) and 1000 W/m^2, (K_t) is the short circuit current per temperature coefficients, (Δt) is the difference between the normal and actual temperatures, and (G_n, G) are the normal irradiation and the irradation of the panel surface respectivly.

2.6.2 Photovoltaic panels (PV panels) Boost Converter Circuit

The boost converter is a DC-DC switch-mode converter where the output voltage is greater than the input voltage. The term steps up converter is based on the step-up the input voltage derived from the operation of converting to a high level than its input. By the law of energy conservation, the input power must be equal to the output power (assuming no circuit losses) (Laguado-Serrano, et al., 2019).

The theory of boost converter operation is depended whether the inductor in the input circuit resists abrupt changes in input current, it means the input current coming from PV panels is variable in the daytime, and the peak of radiation tending to increase of power, therefore should be the choice of the suitable inductor. When the switch is a turn-on, the inductor stores energy on magnetic energy form and discharges it when the switch has turned off, as illustrated in Figure (9) and Figure (10).

The output circuit capacitor is supposed to have a high enough value to make the RC circuit's time fixed high at the output level. Compared to the switching cycle, the large time constant ensures a fixed output voltage.

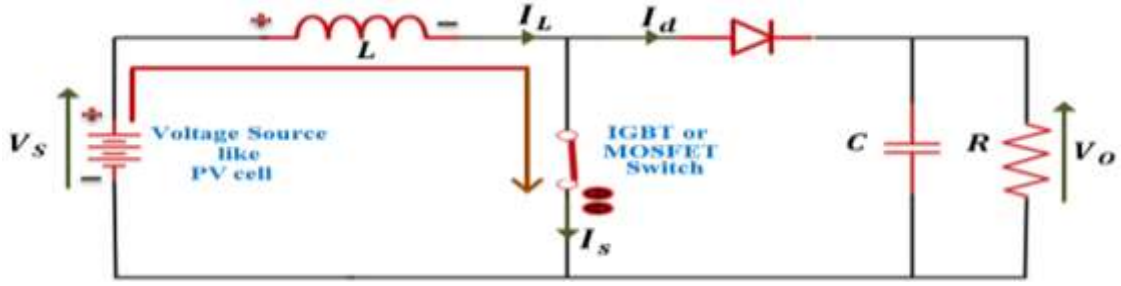

Figure 9. Show the principle turn-on operation of boost converter switch (Muhammad, 2011).

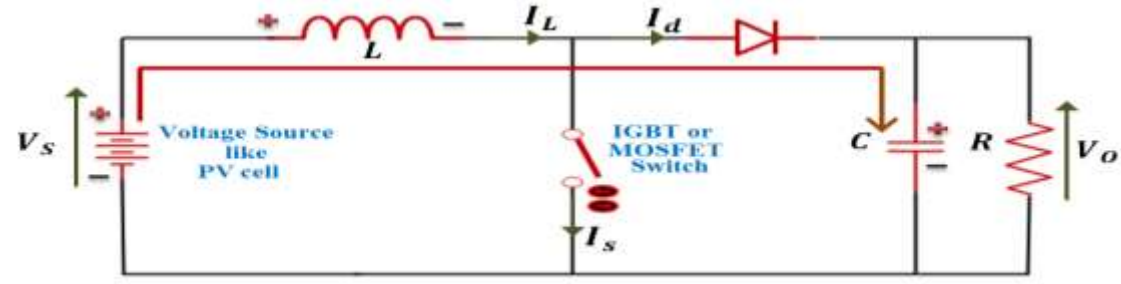

Figure 10. Show the principle turn-off operation of boost converter switch (Muhammad, 2011).

When a boost converter operates in continuous mode, the current through the inductor never falls to zero.

Figure (11) shows the inductor current and voltage waveforms of the converter operating in continuous mode. In steady-state, the DC (average) voltage across the inductor must be zero so that the inductor returns the same state after each cycle, because the voltage across the inductor is proportional to the rate of change of current through the inductor (Javier and Raul, 2004).

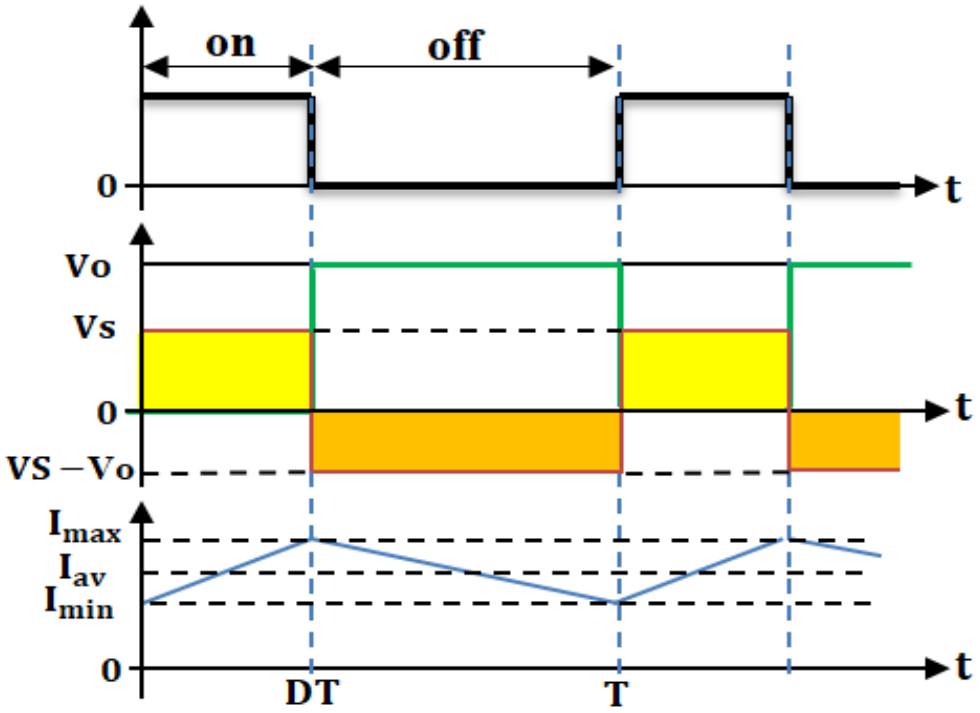

Figure 11. The waveforms of the boost converter in continuous mode .

The mathematical representation of the boost converter in the continuous mode can be obtain from equations below (Javier and Raul, 2004):

$$VS = (1 - D)Vo \qquad (2.26)$$

Where: VS is the input voltage of the PV cell or batteries, Vo is the boost converter output voltage, D is the duty cycle of IGBT. Two techniques are used to evaluate the value of duty cycle, pulse width modulation technique (PWM), and a maximum power point tracking (MPPT) which is used with photovoltaic (Deepak et al., 2015). When the switch is turn-on, the input voltage (VS) appear across the inductor, which causes a change in load current (I_L) flow through the inductor during a time period given by the following equation.

$$\frac{\Delta I_L}{\Delta t} = \frac{VS}{L_1} \tag{2.27}$$

where L_1 is the inductor of coil. At the end of turn-on period, the value of I_L increases, as described by equation (2.28).

$$\Delta I_{L.ON} = \frac{1}{L_1}\int_0^{DT} VSdt = \frac{DT}{L_1}VS \tag{2.28}$$

Where: (D) and (T) are the duty cycle and turn-on switch period respectively, I_L is the inductor current. A large value of capacitor is chosen to remain a constant output voltage.

$$Vo - VS = L_1\frac{dI_L}{dt} \tag{2.29}$$

during the turn-off period of switch, the (I_L) pass through the load. A high-value capacitor is chosen to ensure a fixed or stable output voltage of the boost converter. ($I_{L.OFF}$) value can be calculated by Integral the equation (2.30).

$$\Delta I_{L.OFF} = \int_{DT}^{T}\frac{(VS - Vo)dt}{L_1} = \frac{(VS - Vo)(1 - D)T}{L_1} \tag{2.30}$$

Now, substituting equations (2.26) and (2.29) to find the duty cycle, and illustrated by equations bellow (Javier and Raul, 2004):

$$\Delta I_{L.ON} + \Delta I_{L.OFF} = 0 \tag{2.31}$$

$$\frac{DT}{L_1}VS + \frac{(VS - Vo)(1 - D)T}{L_1} = 0 \tag{2.32}$$

$$\frac{Vo}{VS} = \frac{1}{1 - D} \tag{2.33}$$

$$D = 1 - \frac{VS}{Vo} \tag{2.34}$$

Now, to calculate the value of L_1 from equation (2.35) (Javier and Raul, 2004).

$$L_1 = \frac{D(1 - D)^2R}{2F_{sw}} \tag{2.35}$$

Where: (F_{sw}) is the switch frequency of the boost converter.

2.6.3 Maximum power point tracking (MPPT)

The duty cycle is required to select a suitable pulse to trigger the IGBT or MOSFET switch in the boost converter circuit. There are two methods used to turn ON/OFF power electronic switch, the pulse width modulation (PWM), and the maximum power point tracking (MPPT) (Laguado-Serrano, et al., 2019). A decision about the selection in which one of two approaches depends on the type of input DC source. If the DC input source is fed from batteries, the designers are selecting the PWM technique, where the dc has remained approximately constant and the discharge is linearity. While if the dc input source is fed from photovoltaic cells where the nature of this voltage is considered from variable type because variable radiation of the solar and temperature also, therefore MPPT technique preferred to be chosen. The MPPT is applied to achieve the maximum power of these systems.

There are several methods used to represent the MPPT in order to obtain a maximizing for the PV cells generated power as explained below (Shusmita, et al., 2012):

- **i.** Constant voltage method (CV).
- **ii.** Open Circuit Voltage method (OCV).
- **iii.** Short Circuit Current method (SCC).
- **iv.** Perturb and Observe method (P& O).
- **v.** Incremental Conductance method (INC).

The constant voltage method just deals with low radiation of solar, so it is considered one of the most important disadvantages of this method. The open-circuit voltage method not accurate and may not operate exactly at MPP and slower response as maximum point voltage is proportional to the open-circuit voltage, the short circuit current method, it is not always accurate, low efficiency. The Perturb and Observe method cannot determine when it has reached the MPP under steady-state operation, the output power oscillates around the MPP. The Incremental Conductance method can determine the maximum power point without oscillating around this value, this Benefit is considered better than from the methods above, therefore in this thesis has been used (Shusmita, et al., 2012).

2.6.3.1 Incremental Conductance method

The incremental conductance method (INC) method, is based on the assumption that only the slope of the PV array power curve equal zero, in this case, will get the maximum power point (MPP). Where if the power at the left side of the curve here needs to increase the voltage to arrive MPP. And if the power on the right side of the curve, here needs the voltage decrease to return to MPP. This approach can understand from the curve in Figure (12) and with necessary equations:

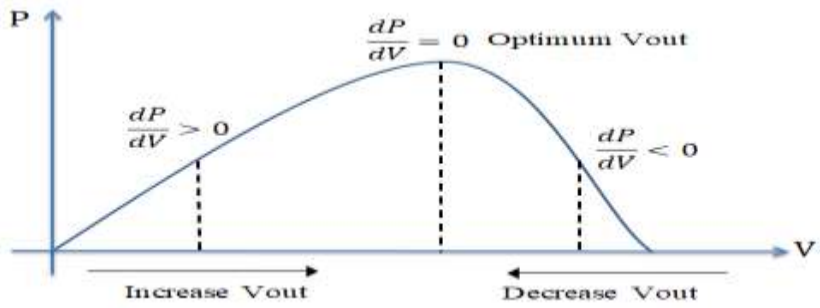

Figure 12. P-V curve of INC (Shusmita, et al., 2012)

$$\frac{dP}{dV} = 0 \text{ , at MPP} \tag{2.36}$$

$$\frac{dP}{dV} > 0 \text{ , at left MPP} \tag{2.37}$$

$$\frac{dP}{dV} < 0 \text{ , at right MPP} \tag{2.38}$$

To link the concept (INC) with the mechanism of work and to clarify by the following equations (Shusmita, 2012; Salah, 2015):

Since $\frac{dP}{dV} = \frac{d(IV)}{dV}$, thererfore

$$\frac{dP}{dV} = \frac{d(IV)}{dV} = I + V\frac{dI}{dV} = I + V\frac{\Delta I}{\Delta V} \tag{2.39}$$

$$\frac{dI_{pv}}{dV_{pv}} = \frac{-I_{pv}}{V_{pv}} \text{ at the MPP} \tag{2.40}$$

$$\frac{dI_{pv}}{dV_{pv}} => \frac{-I_{pv}}{V_{pv}} \text{ at the left of the MPP} \tag{2.41}$$

$$\frac{dI_{pv}}{dV_{pv}} =< \frac{-I_{pv}}{V_{pv}} \text{ at the right of the MPP} \tag{2.42}$$

Where: (V_{pv} , I_{pv}) are the voltage and current of PV respectively, (dV_{pv}) and (dI_{pv}) are derivative value of voltage and current respectively. The maximum point of

power (MPP) is obtained when the derivative equal zero as in the equation (2.69). If the power is less than the MPP, the V_{pv} value must be increased to MPP value according to the equation (2.70). If the power is much than the MPP, the V_{pv} value must be decreased to MPP value according to the equation (2.71).

2.7 Bi-directional (Buck-Boost) Converter

This Buck-Boost converter is a simple DC-DC bi-directional converter circuit, as to obtain in Figures (13) into (2.14). It is an anti-parallel combination of the two buck and boost converters. During the boost (step-up) stage, the switch S1 is a turn-on in the interval (D_bT_b) whereas, switch S2 is a turn-off in this mode. During the step-down mode, the switch S2 is turn-on during the interval $(1 - D_b)T_b$, while the switch S1 still in off-state during this mode (Akhilesh, et al, 2017). Two types of switches have used in bi-directional converter IGBT. Small dead time has added between the two modes of Buck-Boost operation (Daniel and Filip, 2018).

2.7.1 Mathematical Analysis of (Buck-Boost) converter

As stated earlier the Buck-Boost converter operation includes two modes, buck and boost modes (Daniel and Filip, 2018):

2.7.1.1 Boost Mode

In the boost mode, the batteries in the bi-directional circuit is discharging its power in the load (dc-link capacitor voltage of DSTATCOM) in this work (Sarina and Fangxing, 2014). The boost can be explained in two stages, shown in Figure 2.13. The mathematical analysis of this mode is given in the following equations (Daniel and Filip, 2018):

First, at the switch S1 is a turn-on and S2 is turn-off mode, where the DC-DC circuit behaves like booster as shown in figure (13a) which is given by equation (2.43):

$$0 < t < D_bT_b \tag{2.43}$$

Where (D_b and T_b) are duty cycle and period of switch.

The voltage across the inductor is given by:

$$VL_m = VB = L_M \frac{di_{LM}}{dt} \tag{2.44}$$

Where: VL_m and VB are the voltage across the inductor and the batteries, (L_M) is the inductance of the coil and di_{LM} is the current time variation.

Since (i_{LM}) is increased linearly, therefore the equation can be written:

$$\frac{di_{LM}}{dt} = \frac{\Delta i_{LM}}{D_b T_b} = \frac{VB}{L_M} \quad (2.45)$$

The time variation of the inductor current is explained as follows:

$$\Delta i_{LM1} = \frac{V_s}{L_M} D_b T_b \quad (2.46)$$

In the second stage, the switches S1is turn-off and S2 is turn-on state as shown in Figure (13b) (Daniel and Filip, 2018):

$$D_b T_b < t < T_b \quad (2.47)$$

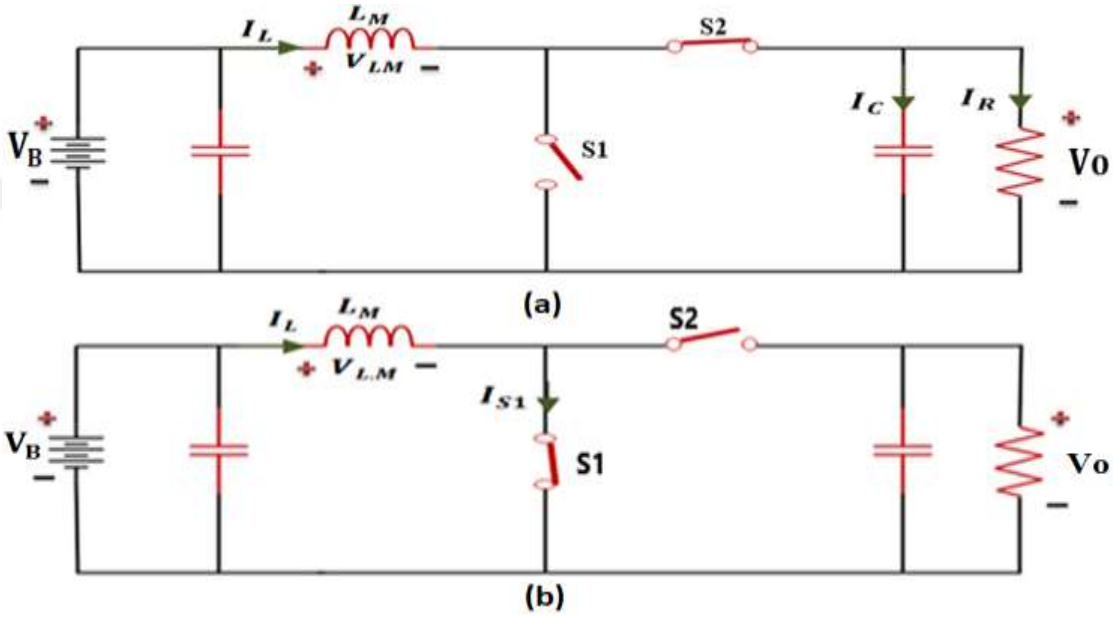

Figure 13. Equivalent circuit of boost mode (Daniel and Filip, 2018).

If the S2 is a turn-on, the and is pass through the load, at this mode, the current in the inductor decreases, as shown in equation (2.48).

$$VL_M = VB - V_O = L_M \frac{di_{LM}}{dt} \quad (2.48)$$

Where: V_O is the output voltage of the boost converter.

Since i_{LM} decrease linearity, then the equation becomes as follow:

$$\frac{di_{LM}}{dt} = \frac{\Delta i_{LM}}{(1 - D_b)T_b} = \frac{VB - V_O}{L_M} \quad (2.49)$$

The i_{LM} is evaluated using equation (2.50).

$$\Delta i_{LM2} = \frac{Vs - V_O}{L_M} (1 - D_b)T_b \quad (2.50)$$

The total change of the current during complete switching duty equals zero based on equations (2.47) and (2.50).

$$\Delta i_{LM1} + \Delta i_{LM2} = 0 \quad (2.51)$$

Then equation (2.51) can be simplified and written by the following equation:

$$Vo = \frac{1}{1 - D_b} VB \quad (2.52)$$

2.7.1.2 Buck Mode

In this mode, the batteries in the bi-directional circuit is charging from the external supply source (like PV panels) (Sarina and Fangxing, 2014). The operation of buck converter can be explained in two stages, in the first stage S2 is turn-on state and S1 is turn-off state, as shown in "Figure (14a). The mathematical representation of this mode is explained by the following equations (Daniel and Filip, 2018):

$$V_{LM} = \frac{di_L}{dt} L = V_{PV} - V_S \quad (2.53)$$

Where: V_{PV} and Vs are the voltages from an external source and batteries. The total significant change in the buck current may be described using the following equation:

$$\frac{\Delta I_{L.ON}}{\Delta T1} = \frac{V_{PV} - V_S}{L_M} \quad (2.54)$$

Where: $\Delta T1$ is calculated from the duty cycle of the first stage and equal $D_b T_b$.

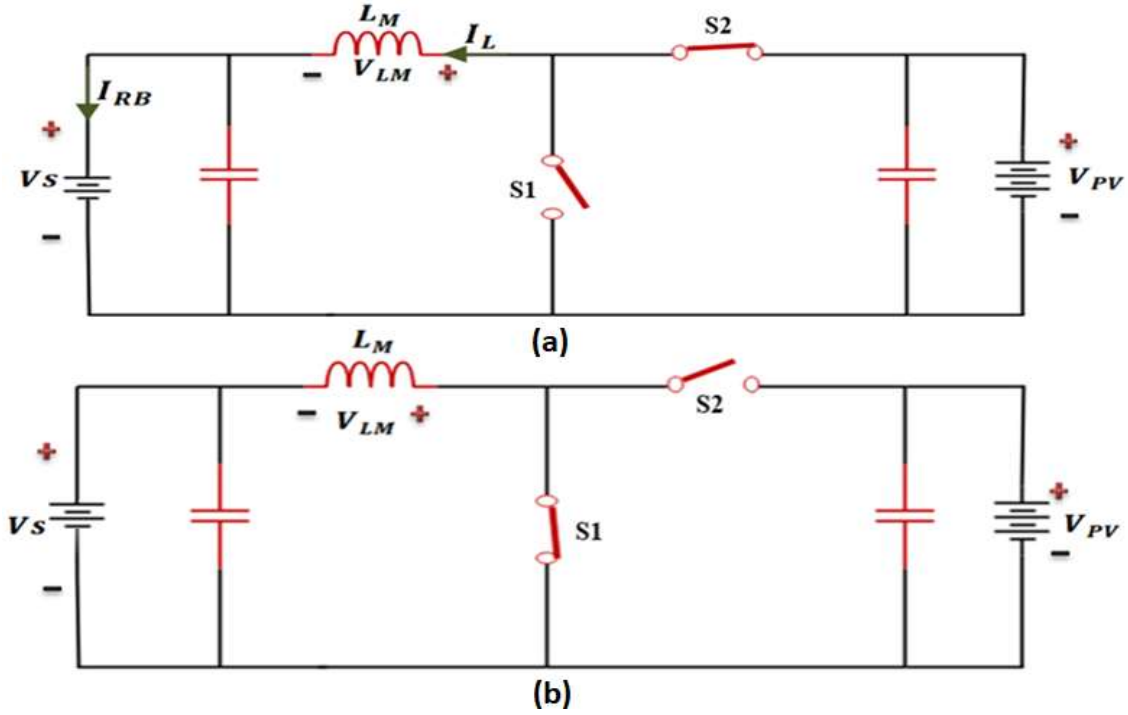

Figure 14. Equivalent circuit of buck converter (Daniel and Filip, 2018).

In the second stage, S2 is turn-off position while S1 is turn-on position as shown in Figure (13b). In equation (2.55), the V_{LM} is negative due to of revers the direction of inductor current.

$$V_{LM} = -V_s \tag{2.55}$$

$$\frac{\Delta I_{L.OFF}}{\Delta T2} = \frac{-V_s}{L_M} \tag{2.56}$$

Where: $(\Delta T2)$ is the second phase duty where it is calculated using $(1 - D_b)T_b$ term. Under steady-state operation, the change in the current should be equal zero, as explained in equation (2.57) (Daniel and Filip, 2018):

$$\Delta I_{L.ON} + \Delta I_{L.OFF} = 0 \tag{2.57}$$

Then the (V_S) is written as follows:

$$\frac{V_{PV} - V_S}{L_M} \Delta T1 + \frac{-V_s}{L_M} \Delta T2 = 0 \tag{2.58}$$

$$V_S = D_b \, V_{PV} \tag{2.59}$$

Now, to calculate the value of L_M from equation (2.60) (Daniel, 2018; Chi-Seng, 2014).

$$L_M = \frac{{V_S}^2 \, (V_{PV} - V_S)}{R_{ind}. F_{sw}. I_{PV}. {V_{PV}}^2} \tag{2.60}$$

Where: R_{ind} and F_{sw} are the maximum current ripple 15%, and the switching frequency 10kHz respectively.

CHAPTER THREE
DESIGN AND SIMULATION OF DSTATCOM

3.1 INTRODUCTION

Each concept must first undergo a logical analysis and simulation based on accurate scientific principles; this is accomplished using sophisticated computer tools such (as MatLab). It can also be said that the Matlab program is one of the most prominent programs in the representation of scientific and engineering ideas because it provides a working environment close to the real reality. It is effectively supported in the areas of representation by blocks diagram and programming codes to obtain the required result for solving systems problems. Therefore, it is used in complete system modeling of the Modified DSTATCOM to obtain compensation active and reactive power of systems in order to improvement a power quality.

3.2 Simulator Scheme of Model

Figure (15) shows the general structure of the power distribution system which has been represented in the present work, which is a generator, transmission line, and nonlinear load. DSTATCOM is connecting between the grid and the nonlinear load. The type of source is three-phase voltage to ground, the type of load is three phases nonlinear, was obtained from a three-phase rectifier loaded by inductance and resistance connected in series. Also, the structure illustrates the location of the PV system (PV panels and batteries) on the dc-channel for DSTATCOM, and the parameters of the system have obtained from Table 1.

Table 1. Parameters of system

Parameters	Values
Three-phase voltage and frequency of the grid	415V, 50Hz
Resistance and Impedance of load	130Ω, 20 mH
Line Impedance (Z)	0.01 Ω, 0.2 mH
Ripple filter (Rf, Cf)	10 Ω, 12.5 uf

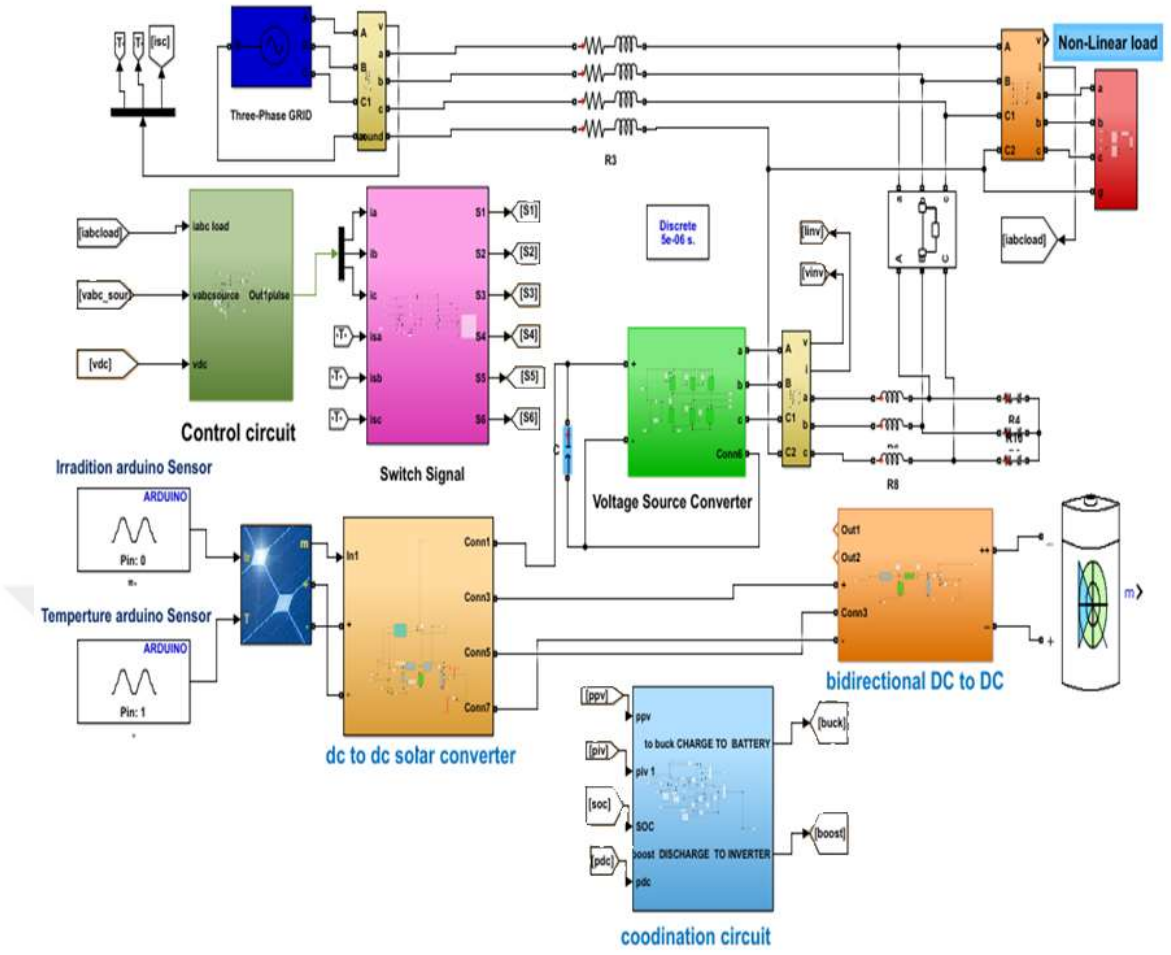

Figure 15. Schematic Diagram of power system with DSTATCOM.

The mathematical equations of the main model.1a shown in Figure (15) are given as follow:

The instantaneous per-phase voltage of the point common coupling (V_{PCC}) (Bhim, et al., 2004).

$$\begin{bmatrix} V_{ac} \\ V_{bc} \\ V_{cc} \end{bmatrix} = \sqrt{\frac{2}{3}} V_S \begin{bmatrix} \sin wt \\ \sin(wt - \frac{2\pi}{3}) \\ \sin(wt + \frac{2\pi}{3}) \end{bmatrix} \quad (3.1)$$

Where: V_S is the rms voltage of PCC voltage, the V_{ac}, V_{bc} and V_{cc} are the voltages of PCC respectively.

Applying Kirchhoff's voltage law on the V_{PCC} and the output voltage of the inverter give the following equations:

$$R_1\, i_a + L_1 \frac{di_a}{dt} = V_{Sa} - V_{Ca} \tag{3.2}$$

$$R_2\, i_b + L_2 \frac{di_b}{dt} = V_{Sb} - V_{Cb} \tag{3.3}$$

$$R_3\, i_b + L_1 \frac{di_c}{dt} = V_{Sc} - V_{Cc} \tag{3.4}$$

Where: V_{Sa} is the grid phase A voltage at PCC V_{Ca} is the phase A output voltage of the DSTATCOM equations (3.2) to (3.4) can be written in matrix form:

$$\frac{d}{dt}\begin{bmatrix} i_a \\ i_b \\ i_c \end{bmatrix} = \begin{bmatrix} R_1/L_1 & 0 & 0 \\ 0 & R_2/L_2 & 0 \\ 0 & 0 & R_3/L_3 \end{bmatrix}\begin{bmatrix} i_a \\ i_b \\ i_c \end{bmatrix} + \frac{1}{L_1}\begin{bmatrix} V_{Sa} - V_{Ca} \\ V_{Sb} - V_{Cb} \\ V_{Sc} - V_{Cc} \end{bmatrix} \tag{3.5}$$

Using park' transformation, the equations are written as below (Bhim, et al., 2004):

$$L \frac{di_d}{dt} + Ri_d = V_{Sd} - m\cos\alpha + Lwi_q \tag{3.6}$$

$$L \frac{di_q}{dt} + Ri_q = V_{Sq} - m\sin\alpha + Lwi_q \tag{3.7}$$

Where: (m and w) are the modulation index of voltage source converter and system frequency respectively.(α) is the angle of converter voltage.

$$\frac{d}{dt}\begin{bmatrix} i_d \\ i_q \end{bmatrix} = \begin{bmatrix} -R/L & w \\ -w & -R/L \end{bmatrix}\begin{bmatrix} i_d \\ i_q \end{bmatrix} + \frac{1}{L}\begin{bmatrix} V_{Cd} - V_{Sq} \\ V_{Sd} + V_{Cq} \end{bmatrix} \tag{3.8}$$

$$V_{Cd} = mV_{dc.renewable}\cos\alpha \tag{3.9}$$

$$V_{Cq} = mV_{dc.renewable}\sin\alpha \tag{3.10}$$

Where: ($V_{dc.renewable}$) is the dc voltage from PV panels or batteries.

$$V_{dc.renew}\, I_{dc.renew} = \frac{3}{2}\left(V_{Cd} i_d + V_{Cq} i_q\right) \tag{3.11}$$

By substituting equations (3.1) to (3.11) we will get DSTATCOM model.1a in state space, obtain in equation below (Bhim, et al., 2004):

$$\frac{d}{dt}\begin{bmatrix} i_d \\ i_q \\ V_{dc.renew} \end{bmatrix} = A\begin{bmatrix} i_d \\ i_q \\ V_{dc.renew} \end{bmatrix} - \frac{1}{L}\begin{bmatrix} V_{Sd} \\ 0 \\ 0 \end{bmatrix} \quad (3.12)$$

Where A is given by equation (3.13).

$$A = \begin{bmatrix} \frac{-R}{L} & \omega & -\frac{m}{L}\cos\alpha \\ -\omega & \frac{-R}{L} & \frac{m}{L}\sin\alpha \\ \left(\frac{3}{2}\right)\left(\frac{m}{c}\right)\cos\alpha & \left(\frac{3}{2}\right)\left(\frac{m}{c}\right)\cos\alpha & 0 \end{bmatrix} \quad (3.13)$$

The DSTATCOM output can be controlled by monitoring the current, (i_d), and (i_q) active and reactive components respectively.

3.2.1 Control strategy of Model

The mathematical equation of the control circuit is clarified in equations (2.9) to (2.20) (Marcelo and PE, 2006). The simulation of control circuit is shown in Figure (16).

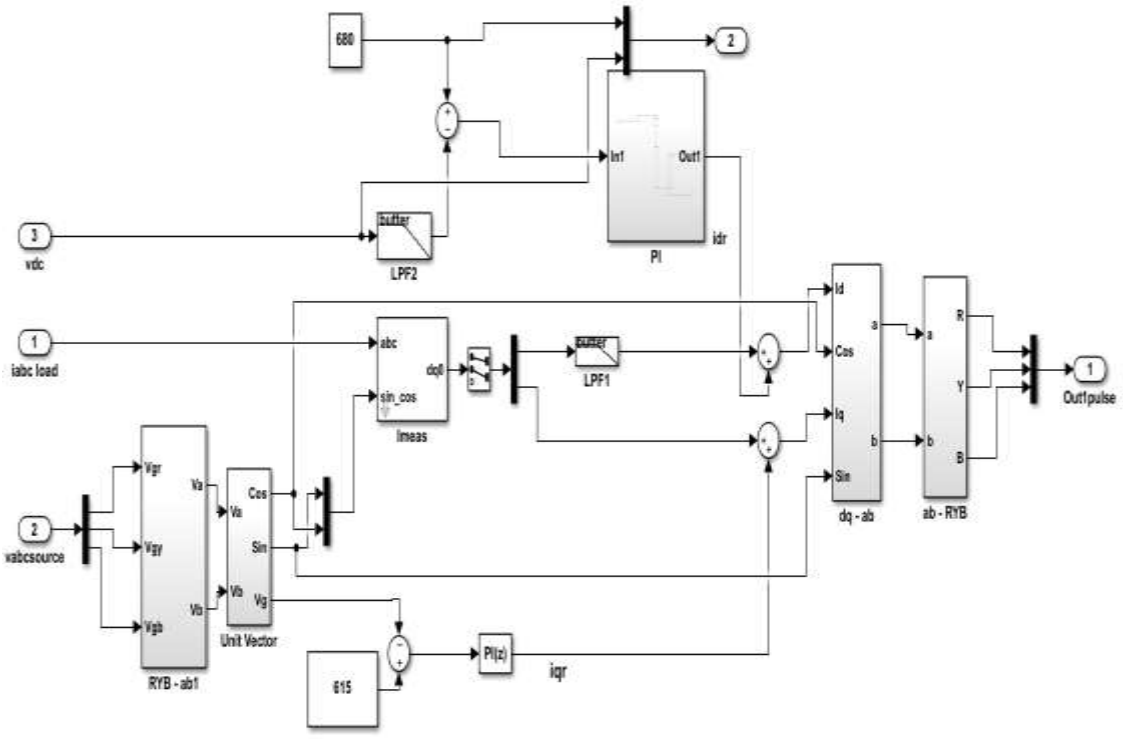

Figure 16. The control circuit of DSTATCOM.

The Clark's transformation from (abc) to (α, β) and clarify in equation (2.10) as shown in Figure (17).

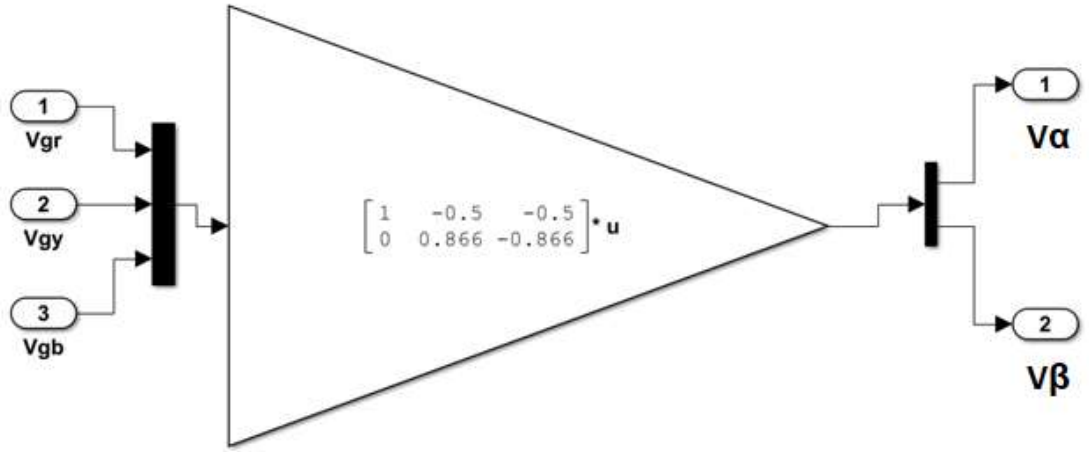

Figure 17. The transformation from abc in to alfa beta.

The unit vector value (VT) and (sinθ, cosθ) are derived from equations (2.11) to (2.13) as shown in Figure (18).

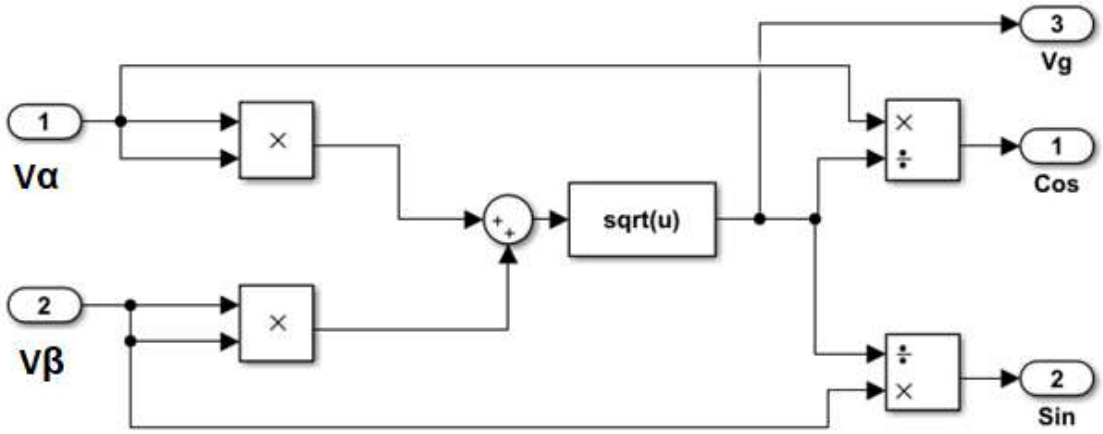

Figure 18. Model of Unit Vector.

The Park's transformation equations are given in Figures (19) and (20), it takes advantage of this conversion to find the value of voltages (VT) and find the values of the trigonometric angle (sinθ, cosθ), is obtained in Figure (19).

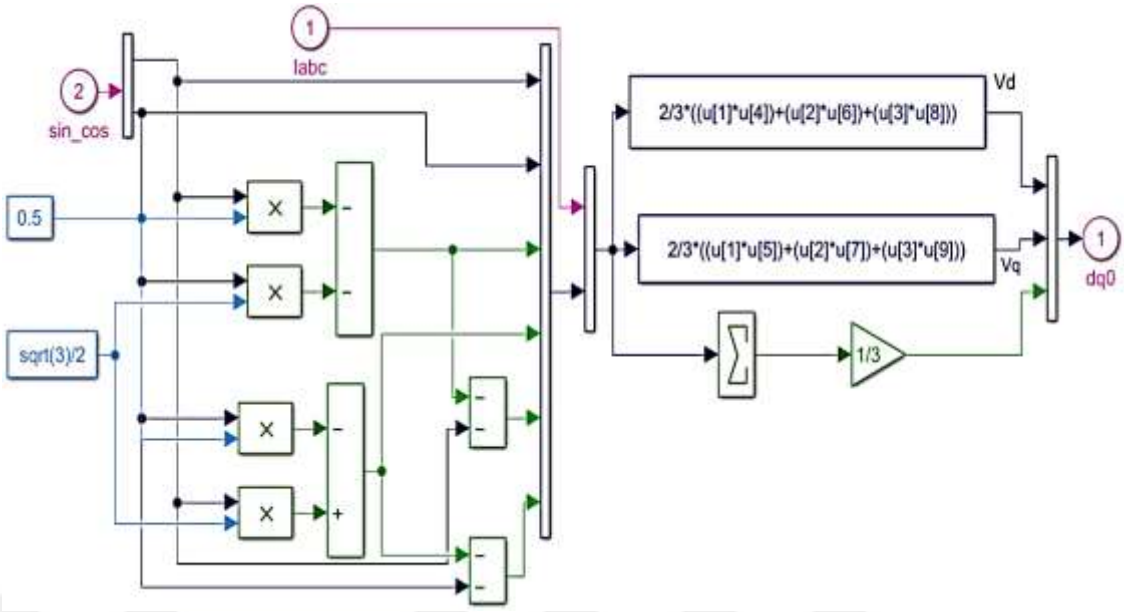

Figure 19. Park transformation from abc to id, iq.

After obtaining (id.ref) and (iq.ref) from equations (2.15) and (2.17) the control circuit compensation, needed back to the abc frame. So that we can compare the modified currents by the control circuit of (DSTATCOM) and the affected currents due to the nonlinear load in the generator, as shown in Figure (20).

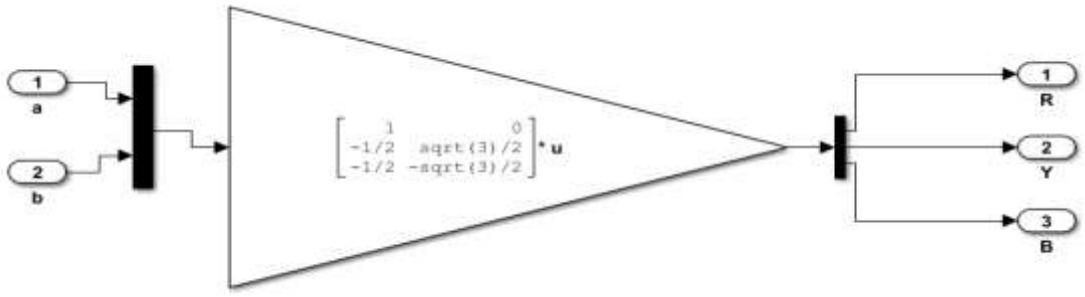

Figure 20. Inverse Park and Clark Transformation.

To generate appropriate pulses for switching DSTATCOM switches, the PWM technique is introduced as shown in Figure (21).

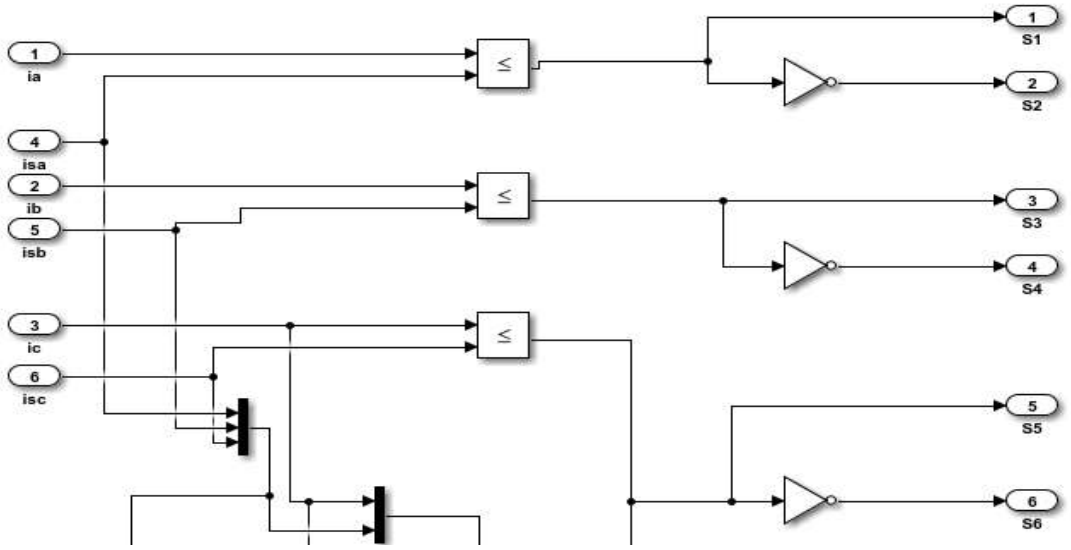

Figure 21. The schematic Diagram of DSTATCOM switching signals.

The equation of the DC voltage regulator (PI.1) is achieved in the (2.14), and the equation of the AC voltage regulator (PI.2) is obtained (2.16). Also, the parameters gains (KI, KP) of (PI.1 and PI.2) have selected from Table 2 by using the trial and error method.

Table 2. Parameters gains of controllers for model

Parameters	Values
DC voltage regulator gain (KP, KI)	4, 3
AC voltage regulator gains (KP, KI)	0.9e-3, 0.15

3.2.2 Design of Voltage Source Converter (VSC)

The voltage source converter (VSC) is the core of DSTATCOM, it consists of six IGBT switches, with a capacitor connected across the input DC side. To calculate the value of the capacitor of DC voltage through the equations below (V Kamatchi and N Rengarajan, 2012):

$$V_{dc.act} = \frac{2\sqrt{2}\, V_{LL}}{\sqrt{3}\, m} \tag{3.14}$$

Where: $V_{dc.act}$ and V_{LL} are the actual DC voltage measured by voltage sensor and the line to line voltage respectively, (m) is the modulation index, also (m) known as is the percentage of carrier waveform on the fundamental.

$$0.5\, C_{dc}\left[\left(V_{dc.ref}^2\right) - \left(V_{dc.act}^2\right)\right] = 3V_{ph}\left(OLFI_{ph}\right)t \tag{3.15}$$

Where: the C_{dc} and $V_{dc.ref}$ are the capacitor of DC link for VSC and the reference DC voltage respectively, (V_{ph}) is the phase voltage of source, (OLF) is over load factor, (I_{ph}) is the phase current, (t) is the less instant time of compensation (V Kamatchi and N Rengarajan, 2012). The schematic diagram of voltage source converter is shown in Figure (3.8).

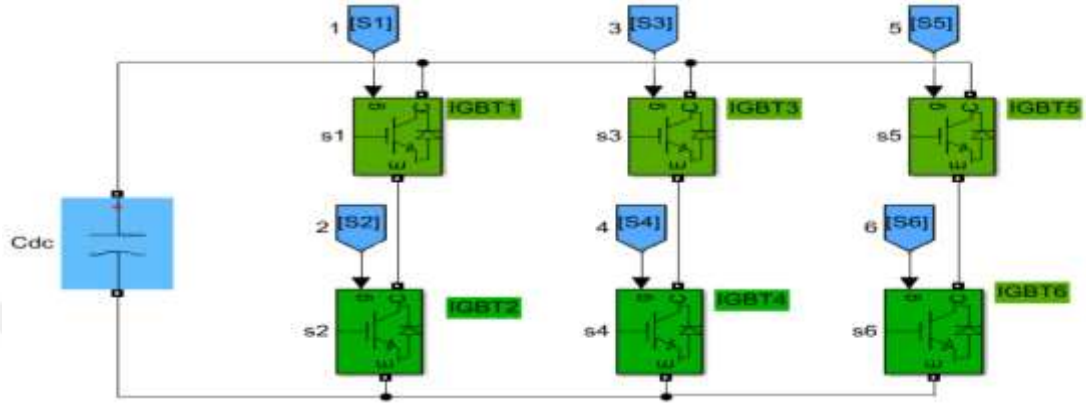

Figure 22. Schematic diagram of voltage source converter (VSC) of DSTATCOM.

The coupling inductance (L) between DSTATCOM and PCC which is used to suppress the harmonic components of output voltage can be evaluated by the equation (Bhim, et al., 2004):

$$L = \frac{\sqrt{3} m V_{dc.ref}}{12\ OLF\ f_s\ r(p-p)} \qquad (3.16)$$

Where: $r(p-p)$ is the ripple factor of dc voltage, while (f_s) is the switching converter frequency (Binayak, et al., 2014). The values of parameters are calculated from the equations (3.14) into (3.16) are shown in Table 3.

Table 3. The parameters is calculated from equations (3.14) to (3.16).

Parameters	Values
Capacitor of DC link for VSC (C_{dc})	3000μF,1000V
The reference DC voltage	680V
Over load factor (OLF)	1.2
Modulation index (m)	1
The phase voltage of source (V_{ph})	240V
The phase current (I_{ph})	58.13A
The actual DC voltage ($V_{dc.act}$)	670V
Instant time of compensation (t)	350 μs
The ripple factor of dc voltage	5-15%
The switching converter frequency (f_s)	(10 kHz)
Coupling inductance between DSTATCOM and PCC (L).	3mH

3.2.3 Design of Boost Converter for PV system

The boost converter parameters are evaluated based on equations (2.55) to (2.65) and the MatLab model.1a of the circuit is shown in Figure (23). The value of its parameters is given in Table 4 (V Kamatchi and N Rengarajan, 2012).

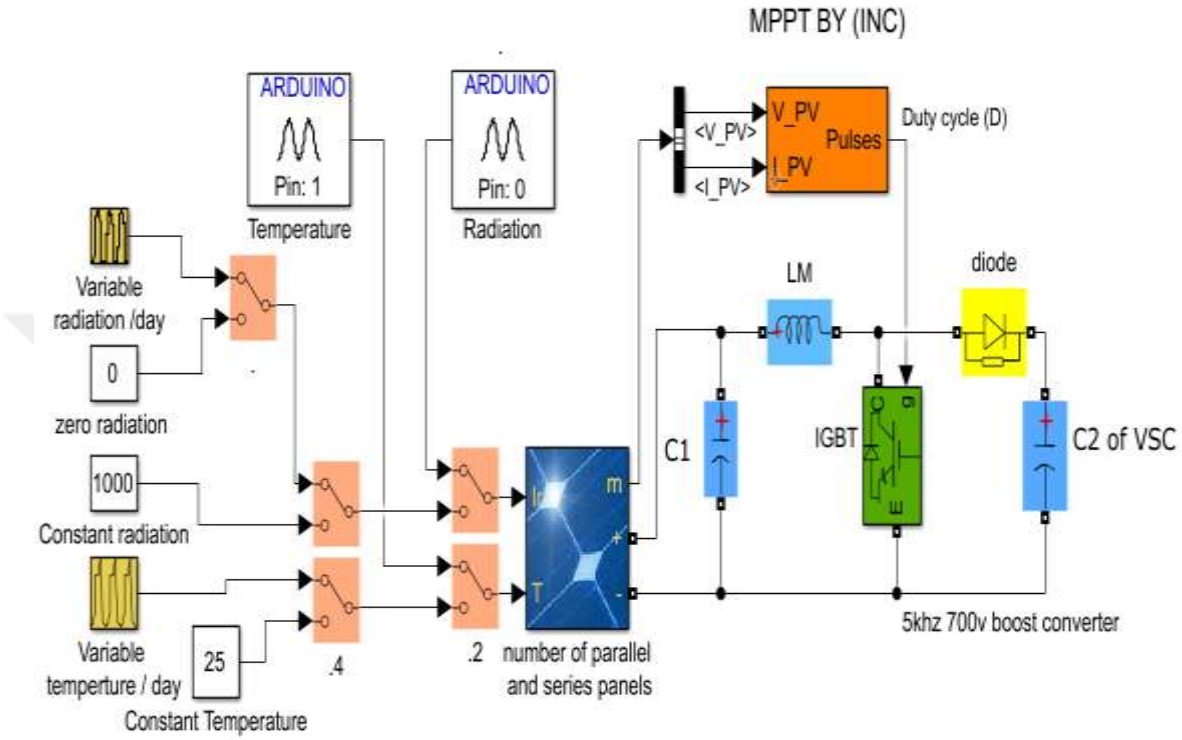

Figure 23. MatLab\Simulink model of boost converter circuit of PV with variable input (radiation and temperature).

Table 4. Parameters of boost converter.

Parameters	Values
Inductor of coil (LM)	0.048mH
Capacitor (C1)	2000 µf
Capacitor (C2) for VSC	This capacitor is the same value as the capacitor mentioned in table 4 and equals 3000 µf

3.2.4 Photovoltaic Module Model

The PV contains many panels (modules) linked in series and in parallel to deliver a suitable voltage and current of operation.

The I-V characteristics is itemized in table 5. The module of PV cell is used in this thesis by Shanghai alex solar energy Science & Technology ALM-170D-24 [37]. To calculate the total power of PV panels generation is obtained from equation (3.17) (Chung and Hsin, 2014).

Table 5. Specifications solar panel model datum at 1000 W/m^2 and 25℃.

Parameters	ALM-170D-24 Data
Maximum Power (W)	170 W
Open circuit voltage Voc (V)	44.2 V
Short circuit current (I_{sh})	5.01 A
Voltage at maximum power point Vmp (V)	35.2 V
Current at maximum power point Imp (A)	4.83 A
Temperature coefficient of short circuit	0.055A/℃
Temperature coefficient of open circuit	- 0.37501V/℃
Number of cells	72

$$PT_{pv} = N_P N_S P_{pv} \quad (3.17)$$

Where: PT_{pv} and P_{pv} are the total power of Photovoltaic cells and the power of each Photovoltaic cell respectively, N_P and N_S are the number of parallel panels of PV and number of the series panels f respectively. In model.1a the PT_{pv} equal 60 kW. The variable radiation and variable temperature are simulated in MatLab\Simulink using a repeating table block while the radiation and temperature are represented by a constant block. The MatLab (2017-2021) Simulink environment provided a connection between Arduino and Simulink, by (supported package for Arduino hardware), as in Figure (24). This feature has been used to measure solar radiation and temperature. The Arduino Mega 2560 has been used to measure the value of radiation of solar by the LDR sensor in addition to record the temperature variation using the KY-013 analog temperature sensor, where consider as a hardware part (San and Zaw, 2018). The hardware is obtained in Figures (25) and (26).

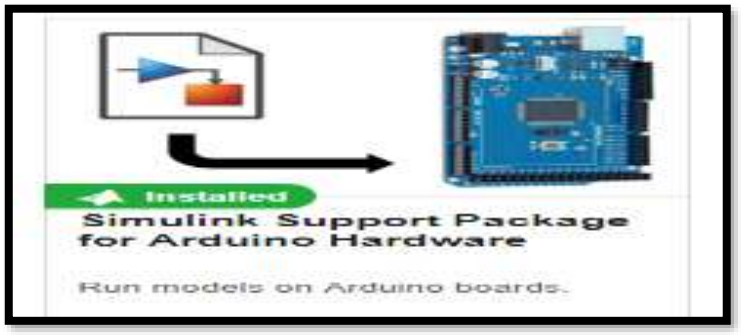

Figure 24. MatLab\Simulink connection with Arduino.

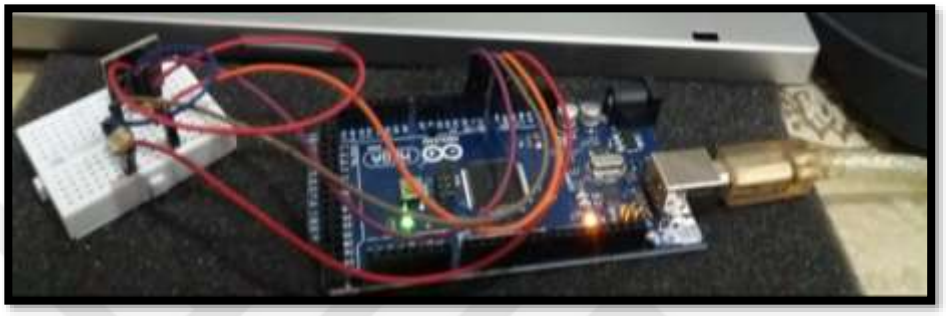

Figure 25. The hardware parts Arduino and sensors.

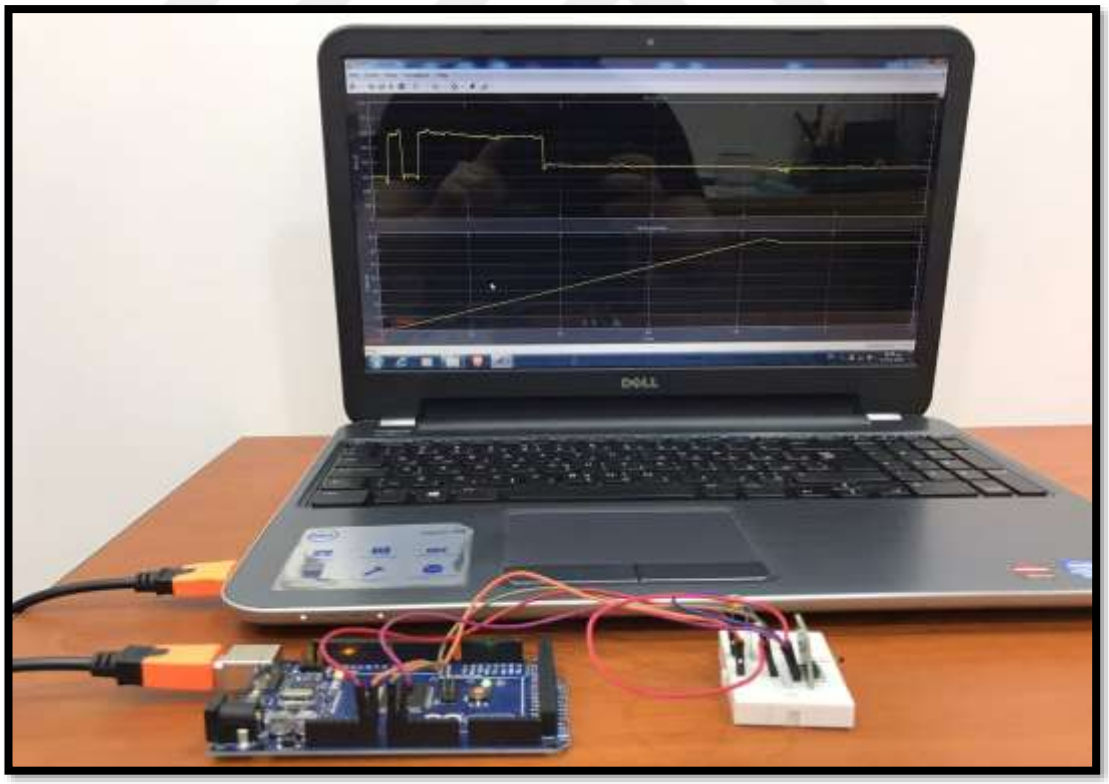

Figure 26. The connection between Arduino and sensors with Simulink.

3.2.5 Modeling of (MPPT) Unit

The Incremental Conductance manner (INC) is one of the good methods for MPPT. The equations of the INC method are obtained by (2.65) into (2.71) (Shusmita, et al., 2012). The INC technique is used for selecting suitable pulses of IGBT switches for VSC as shown in Figure (23). Shows Figure (27) the principle of INC algorithm flow chart.

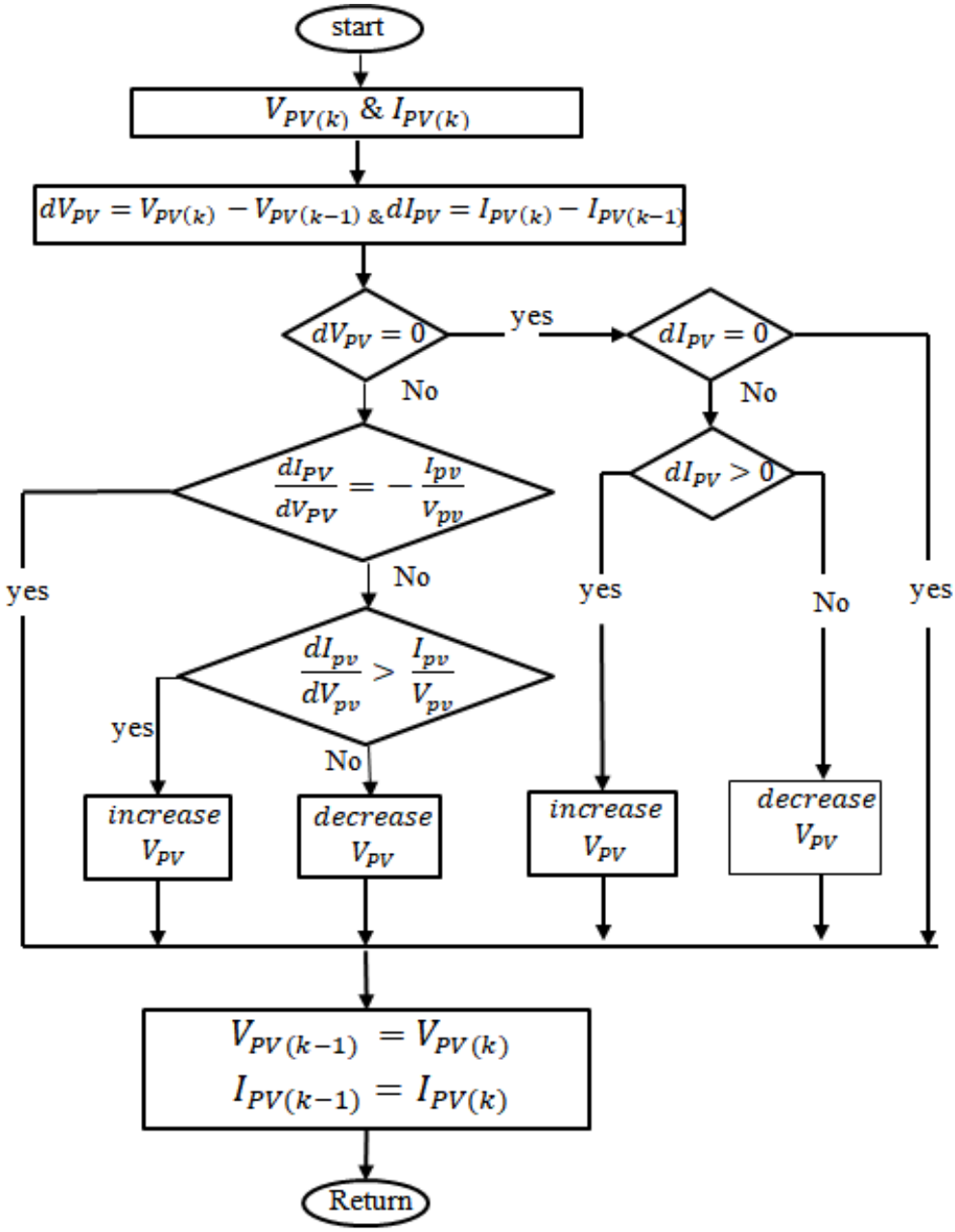

Figure 27. INC flow chart (Pallavee and RK, 2013).

3.2.6 Modeling of Batteries Bi-directional Converter Circuit

The general concept to the hybrid system is completing, when using the buck-boost converter circuit a represented in the bi-directional converter circuit. This circuit is applied to push the excess of the solar module energy to charge the batteries where a buck circuit is a work in this case by turn-ON the Buck of IGBT. When the generating power of the solar module is low or zeroes, the stored batteries energy begins to discharge by turn-ON Boost of IGBT (Daniel and Filip, 2018). The MatLab\Simulink model of the bi-directional converter is build based on equations (2.72) to (2.89) (Daniel and Filip, 2018). As shown in Figure (28). The value of LM equals 60mh and C1 equal 3000uf.

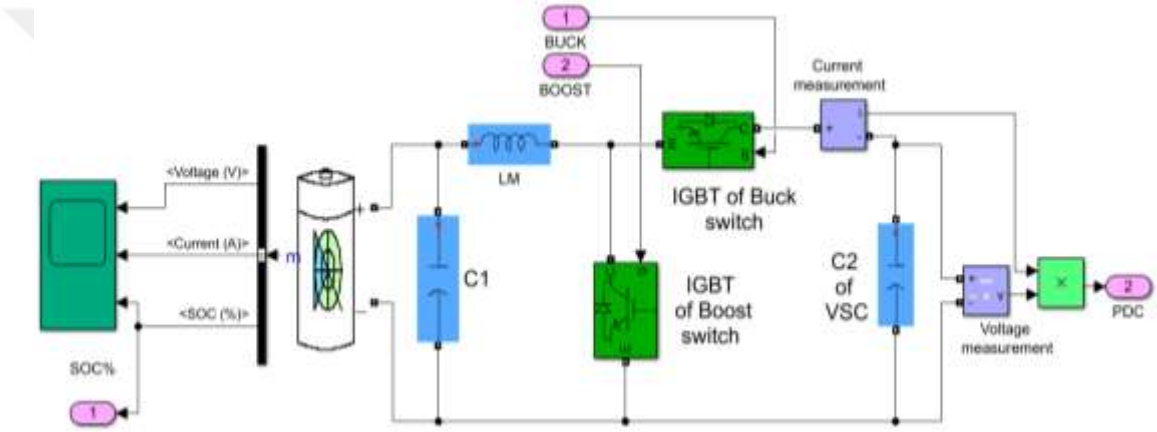

Figure 28. Batteries bi-directional converter circuit.

3.2.6.1 Lead Acid Batteries

The lead-acid batteries used in the present work is the most common type of batteries with hybrid systems. Therefore, the deep-cycle of lead-acid is considered accepted if compare with other types of the batteries (Igor, 2006).

To maintain the batteries life, the control circuit of the coordination circuit has been designed so that the charging state of the batteries does not exceeding 100% from the total charging of the batteries, and the discharging-state is not less than 20% (Metin, 2011). The discharging and charging state of the lead-acid batteries is described by the next set equations (Avjs and Sheldon, 2019):

$$V_{Bat_{dis}} = V_S - Ri - k\frac{Q}{Q - Q(t)}\left(Q(t) + t^f\right) + \exp(t) \qquad (3.18)$$

$$V_{Bat\_ch} = V_S - Ri - \left[k\frac{Q}{Q(t) - 0.1Q}\right] i^f - \left[k\frac{Q}{Q - Q(t)}\right] i^f + \exp(t) \quad (3.19)$$

$$Q(t) = \int i\, d(t) \quad (3.20)$$

Where: $V_{Bat_{dis}}$ and V_{Bat_ch} are the charge and discharge voltages of batteries respectively, (V_S) is the constant voltage of batteries, (k) is the constant for the polarization (V/Ah), (Q) is the capacity of batteries (Ah), $Q(t)$ is the energy of batteries (W/h) and compute from equation (3.19), (i) is the instant batteries current, (i^f) is the current filter, and (t^f) is the time-filter. Specifications of the batteries is given by table 6.

Table 6. Specification of batteries.

Type of Batteries	Lead_Acid
Normal voltage	550V
Rated capacity	17.5Ah
Initial state of charge	50%

3.2.7 Coordination logical circuit Between PV system

Provided by coordination logical circuit below in Figure (29). The high coordination technique is a technique used to manage the input power of STATCOM from different energy sources. It is introduced in the compensation control circuit to regulate the power of PV, power of the batteries, power of voltage source converter (VSC), and the status of batteries or percentage of charge and discharge of the batteries (SOC%). The SOC% is very important for limiting the values of charge and discharge batteries when used in the application fit practical circuits (Avjs and Sheldon, 2019).

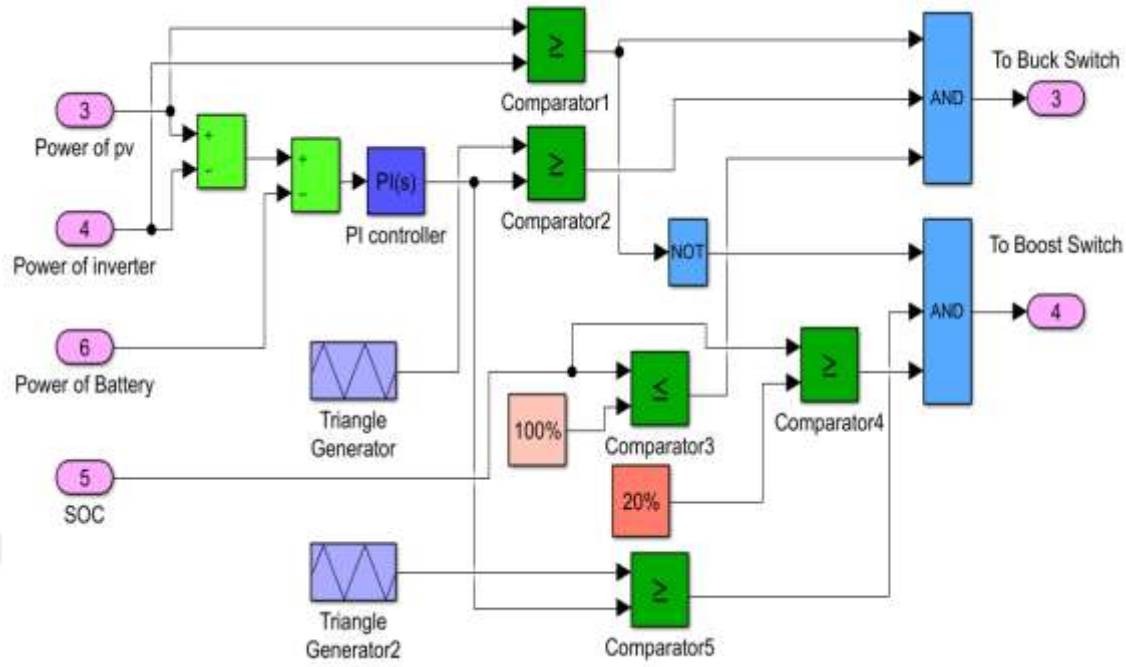

Figure 29. Coordination circuit of battery-PV panels.

If the power of PV is higher than the inverter power then the decision a send into the logic 1 into the AND gate, where, the surplus of power goes to charge the batteries. In this case, the IGBT switch of the Buck circuit is turn-ON.

If the power of PV is low or zero, a comparison is done with the batteries power, and with the state of the percentage charge for batteries (SOC%), then a decision turn-on signal is sent switch of the boost circuit. The PI controller to decrease the error and increase response time to work. The values parameters gain of the PI controller has been found by trial and error method where KI and KP gains are tuning equals $0.8 * 10^{-9}$ and $0.8 * 10^{-8}$ respectively (Avjs and Sheldon, 2019).

CHAPTER FOUR
ANALYSIS AND DISCUSSION SIMULATION RESULTS

4.1 Introduction

This chapter contains a review and discussion of the Simulation results that have been applied to the main model for DSTATCOM. The model of DSTATCOM has been used the PV system (PV and batteries) on the dc-channel of DSTATCOM for power equality improvement like total harmonics distortion (THD%) of current for grid.

4.2 Simulation Results for model

The simulation and results have been applied by MatLab 2018a. A three-phase generator has used with a non-linear load for the case study. The non-linear load was obtained from a three-phase rectifier loaded through RL circuit. The Photovoltaic (PV panels) and batteries have been applied have worked together for the dc-channel of DSTATCOM. This means PV system (PV panels and battery) have fed the dc-channel of VSC for DSTATCOM together. Real time measure is applied on PV panels from the arduino interface on the simulation of MatLab

4.2.1 Case Test

The case test is applied from the generator and Nonlinear load.

Figure 30 shows the three-phase waveform of the generator before compensation when the value of the line voltage is 415v, 50 Hz.

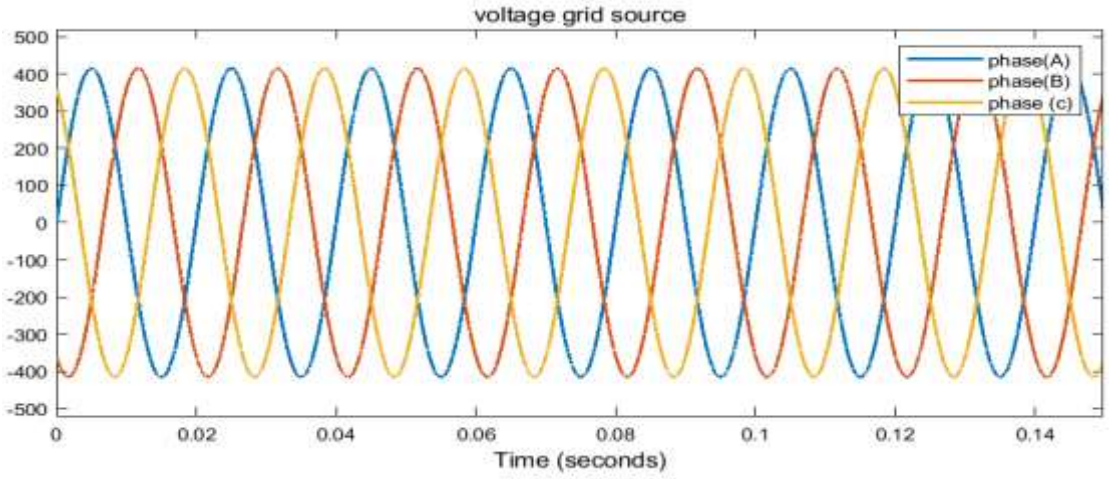

Figure 30. Three phase voltage source of grid (generator).

Figure 31 shows the three-phase current source of the grid before compensation with non-linear load obtained from the three-phase rectifier loaded through RL circuit. It was noted that the value of current source equal 5.3A.

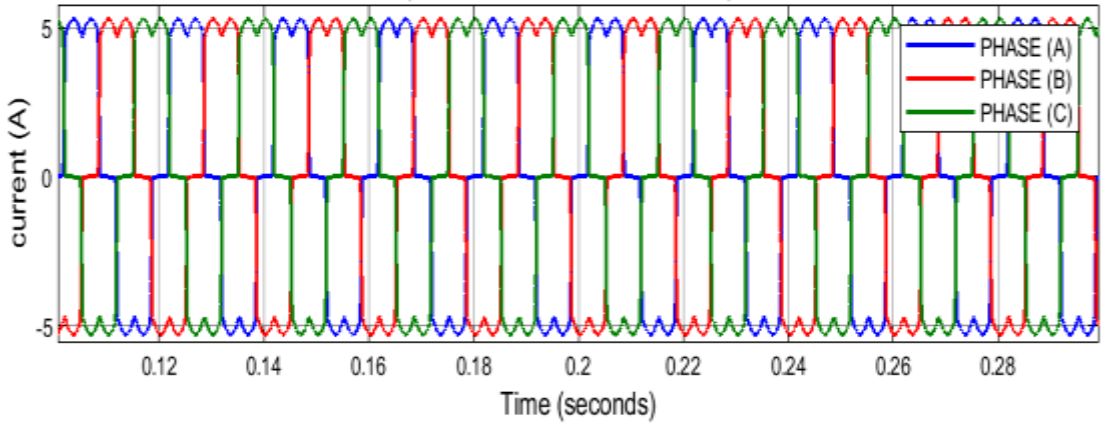

Figure 31. Three phase current source of grid before the compensation.

Figure 32 shows the THD% of three phase current source before compensate the THD =28.25% at the fundamental (50Hz) at 5.608.

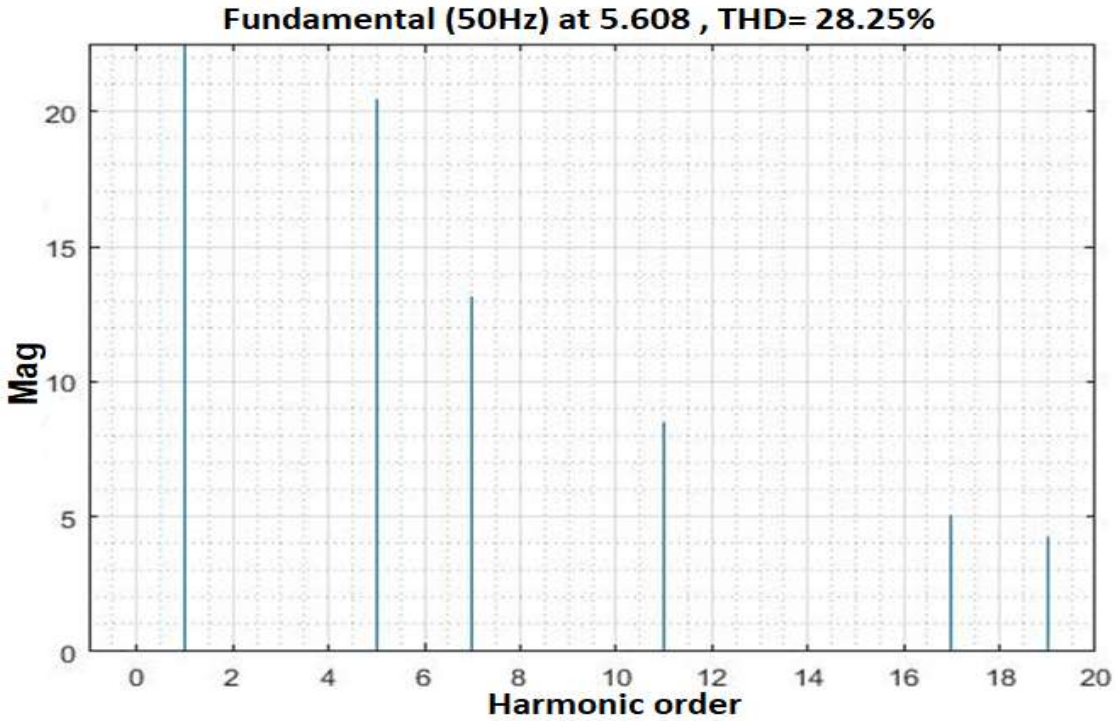

Figure 32. The THD % three phase current source before the compensation.

4.2.2 After Compensation Without PV System on DSTATCOM

Figure 33 three phase current source grid after compensation without PV system on the dc side for DSTATCOM. It was noted that the current of source equal 67A.

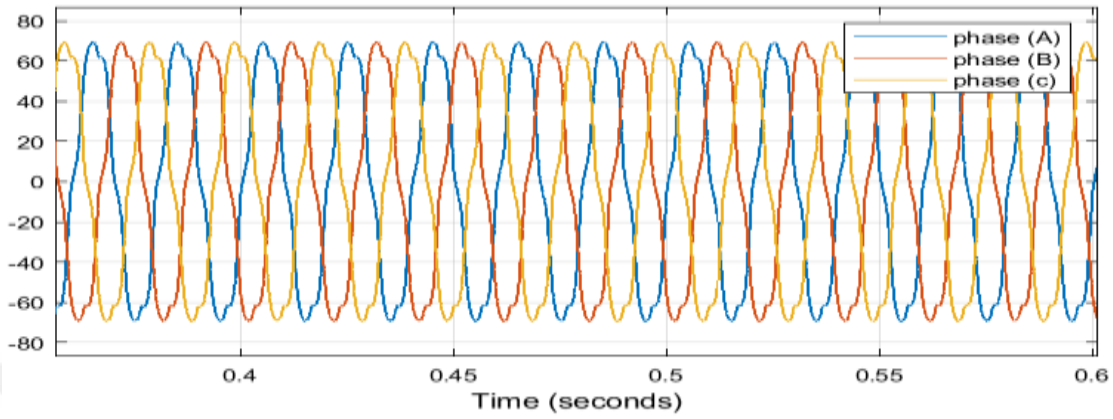

Figure 33. Three phase current source after compensation without PV system.

Figure 34 indicates the THD% after compensation as DSTATCOM operated alone without PV system on the STATCOM.

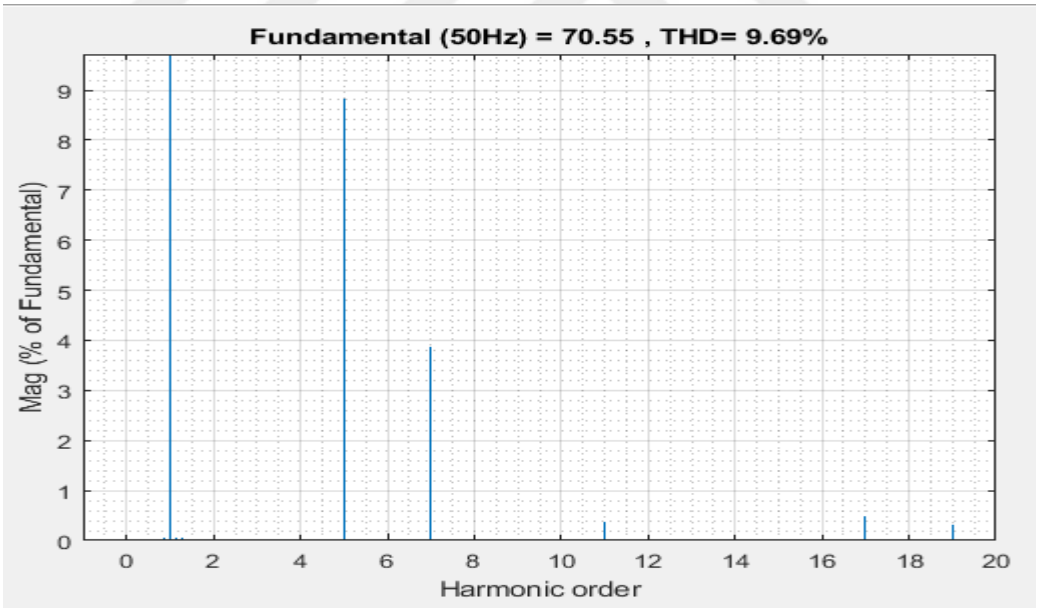

Figure 34. The THD% proportion for current supply source phase (A) after compensation when as DSTATCOM (Alone).

4.2.3 After Compensation with PV system

Now the results after compensation with dc-sources (PV panels and batteries) supply the dc-channel of DSTATCOM. The work has been divided into four situations:

i. Power compensation during the cloudy day (cloudy mode).

ii. Power surplus of panels at day time (high production mode).

i. Power compensation during the cloudy day (cloudy mode):

Sometimes when the climate is cloudy and there is no solar radiation, and therefore the electricity production from the panels is zero. Therefore, the design takes into consideration the cloudy day and the power allowance of the batteries and the grid for a complete day of 24 hours. The status of period time for a cloudy day and temperature is listed in theTable 7.

Table 7. The condition of radiation and temperature for a cloudy daytime.

Time period (Second)	**Time period real (Hour)**	**Radiation of solar** (w/m^2)	**Temperature** (℃)	**Time period (Second)**
0	12 p.m	0	0	0
0.05	1 a.m	0	1	0.05
0.25	5 a.m	20	3	0.25
0.3	6 a.m	30	13	0.3
0.4	8 a.m	35	16	0.4
0.5	10 a.m	40	18	0.5
0.6	12 noon	35	20	0.6
0.7	2 p.m	45	22	0.7
0.8	4 p.m	40	15	0.8
0.9	6 p.m	30	10	0.9
1	8 p.m	5	2	1
1.1	10 p.m	0	1	1.1
1.2	12 p.m	0	0	12

Figure 35 (a) the radiation of solar equal 0 w/m^2, (b) variable temperature, and it noted the low degree for temperature because of cloudy day, (c) the voltage of batteries and notes the voltage down to the 300v because the batteries supplied the dc-link of DSTATCOM (alone), (d) the current of batteries, from the figure notes the current of batteries equal 118A because all of the power demand are taken from the batteries, (d) the status of charge and discharge for the batteries (SOC%), it noted the SOC% decreased for the same cause above and (f) the current supply generator source for phase (A) after compensation.

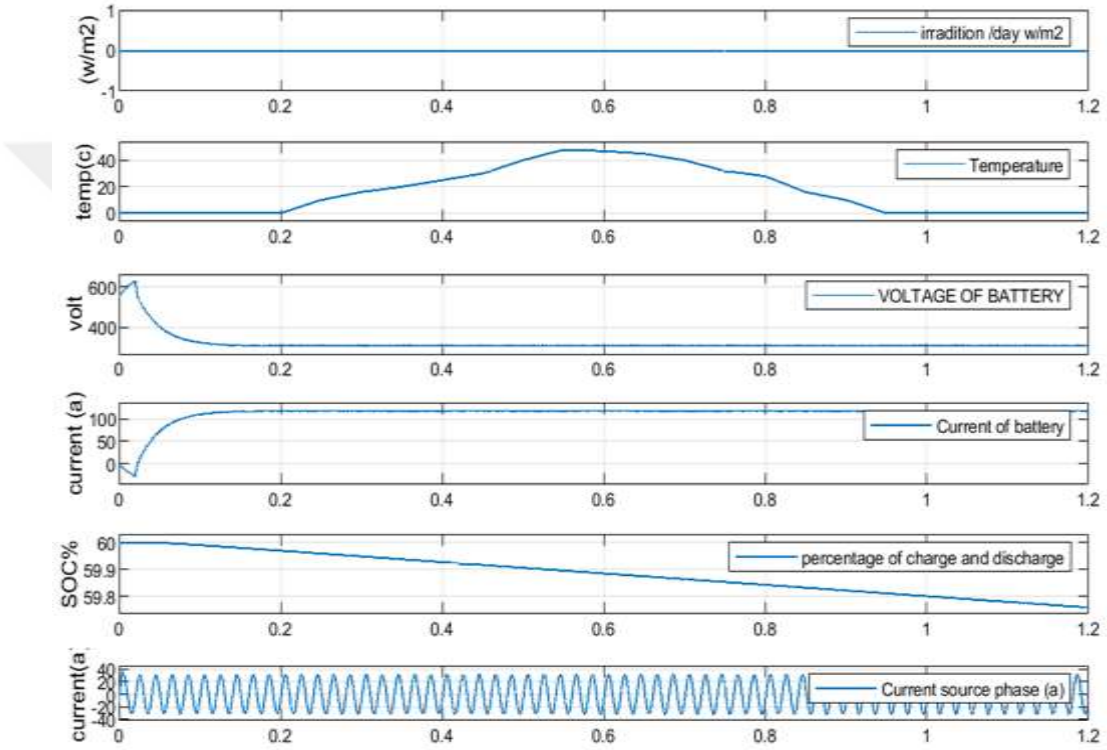

Figure 35. Status for situation1.

Status of multi-sources dc-link of DSTATCOM, PV alone or batteries alone or togethor (PV panels and batteries) with real-time is given in Table 8.

Table 8. The status of batteries alone that supply the DSTATCOM.

Time period (Second)	Time period real (Hour)	Status of (PV)	Status of (batteries)	Hybrid (PV panels and batteries)
0	12 p.m	OFF	ON discharge	OFF
1.2	12 p.m	OFF	ON discharge	OFF

Figure 36 shows the three phase current source after compensation when the batteries supplied the dc link of DSTATCOM (alone).

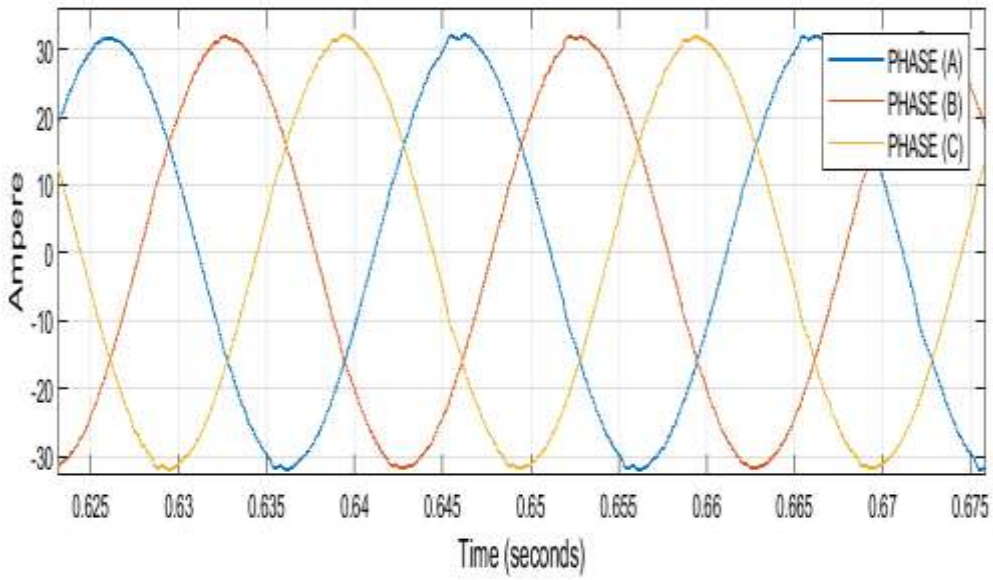

Figure 36. The three phase current supply source after compensation for situation 1.

Figure 37 the THD% of three phase current supply source after compensation when the batteries delivered the dc-link of DSTATCOM (alone).

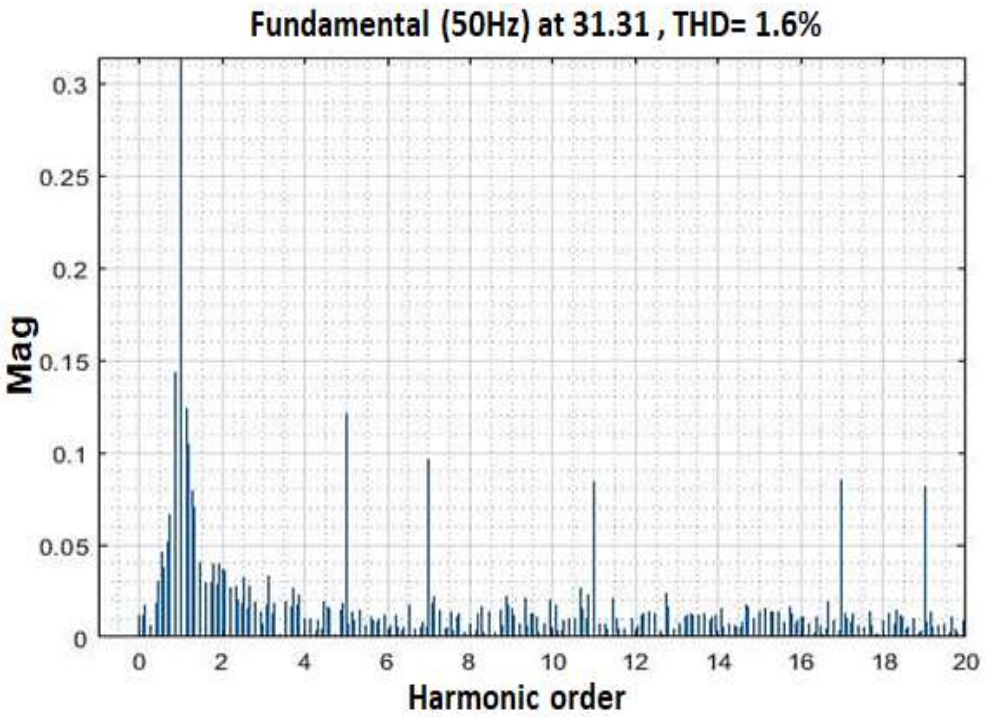

Figure 37. THD% proportion of three phase current supply source of situation1.

Figure 38 shows the power of PV panels and equal 0 kW and the power of batteries equal 32.5kW, it has distributed the active power of DSTATCOM equal 27kW.

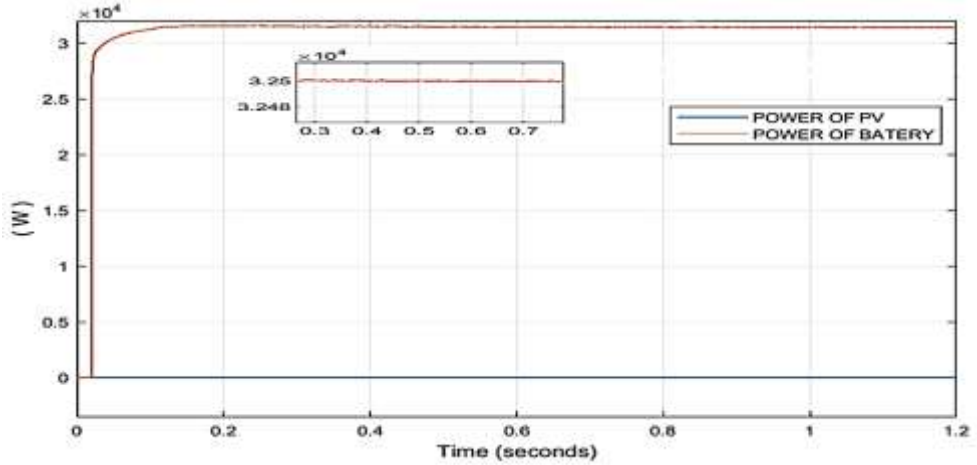

Figure 38. The power of batteries and DSTATCOM .

ii. Power surplus of panels at day time (high production mode):

In this case, the out voltage of the PV panels provides the necessary compensation for the DSTATCOM dc-channel also charging the batteries.The status of period time for 1 day of June as variable radiation and temperature in Table 9.

Table 9. The status of radiation and temperature for one day in June.

Time period (Second)	**Time period real (Hour)**	**Radiation of solar** (w/m^2)	**Temperature** (℃)	**Time period (Second)**
0	12 p.m	0	20	0
0.05	1 a.m	0	19	0.05
0.25	5 a.m	100	22	0.25
0.3	6 a.m	300	25	0.3
0.35	7 a.m	500	30	0.35
0.4	8 a.m	800	35	0.4
0.5	10 a.m	950	40	0.5
0.6	12 noon	1000	48	0.6
0.7	2 p.m	1000	48	0.7
0.8	4 p.m	600	40	0.8
0.85	5 p.m	400	38	0.85
0.9	6 p.m	200	35	0.9
1	8 p.m	0	28	1

Status of multi-sources, PV panels alone or batteries alone or PV system (PV panels and batteries) with real time is given in Table 10.

Table 10. The status of multi-supply PV system (PV and Battery) sources.

Time period (Second)	Real Time period (Hour)	Status of (PV)	Status of (batteries)	PV System
0	12 p.m	OFF	ON discharge	OFF
0.05	1 a.m	OFF	ON discharge	OFF
0.25	5 a.m	ON	ON discharge	ON
0.3	6 a.m	ON	ON discharge	ON
0.4	8 a.m	ON	ON discharge	ON
0.5	10 a.m	ON	ON charge	OFF
0.6	12 noon	ON	ON charge	OFF
0.7	2 p.m	ON	ON charge	OFF
0.8	4 p.m	ON	ON charge	OFF
0.85	5 p.m	ON	ON charge	OFF
0.9	6 p.m	ON	ON discharge	ON
0.95	7 p.m	ON	ON discharge	ON
1	8 p.m	OFF	ON discharge	OFF
1.1	10 p.m	OFF	ON discharge	OFF
1.2	12 p.m	OFF	ON discharge	OFF

The results of situation 3 depend on Table 9 and Table 10.

Figure 39 shows in (a, b) the variable radiation and temperature respectively, (c, d) the voltage and current of batteries respectively, (e) the status of charge and

discharge for batteries, and (f) the current supply generator source for phase (A) after compensation.

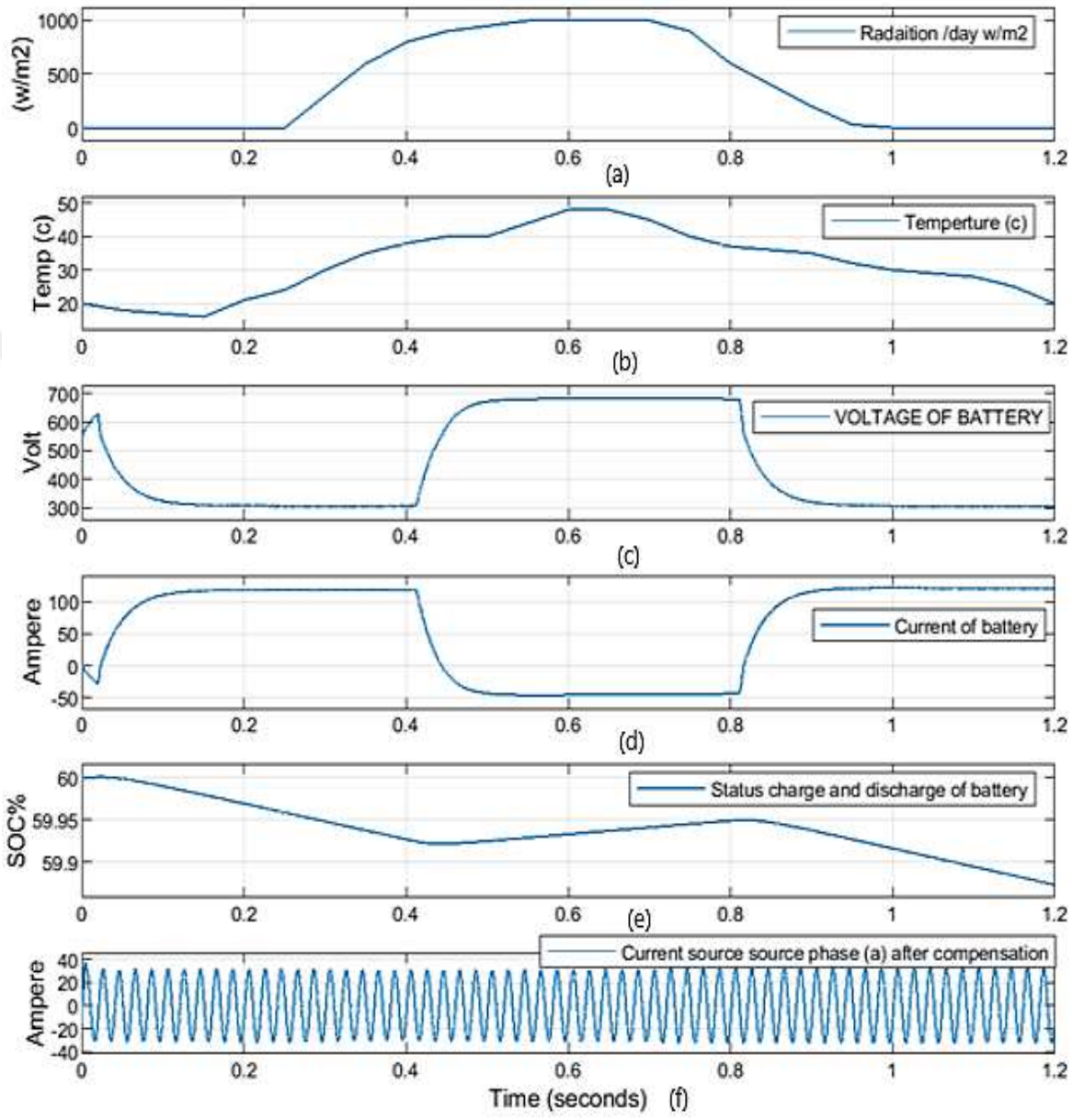

Figure 39. Status of situation 2.

Figure 40 shows the three phase current source after compensation and notes the current source equal 32A.

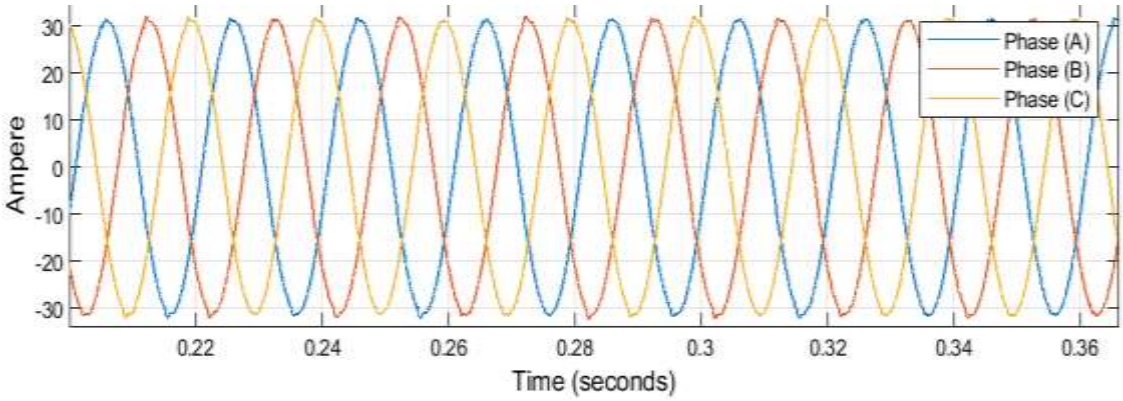

Figure 40. Three phase current supply (source) after compensation for situation 2.

The THD% proportion for the current supply source of phase (A) is obtained in figure 41.

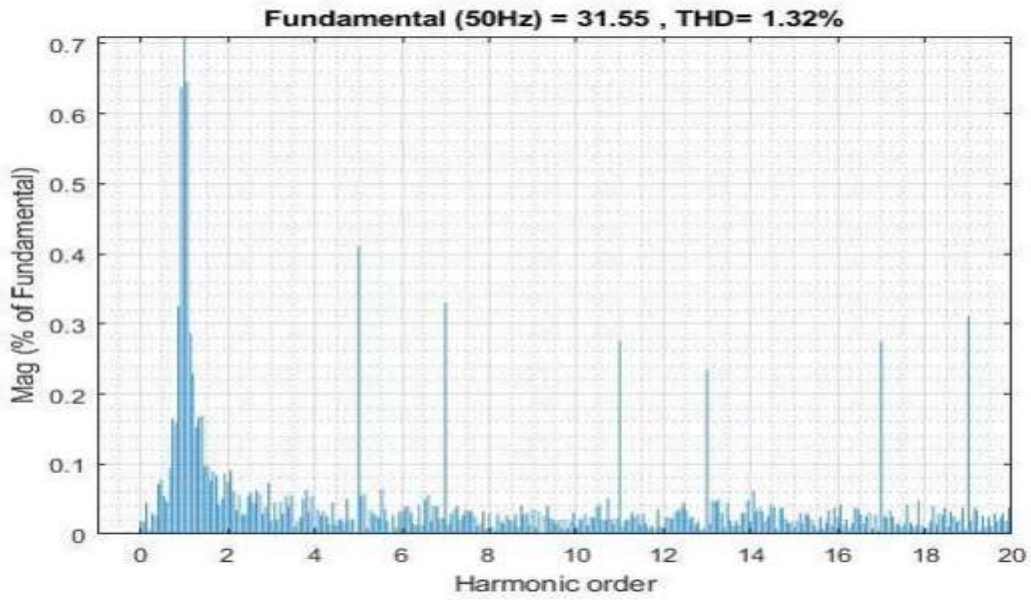

Figure 41. The THD% after compensation of current source phase (A) for situation 2.

Figure 42 shows the power of PV panels and power of the batteries when the high production of solar in the day time. It starts from 0.25s that equal 5 a.m into 0.95s that equal 7 p.m, which is explained in tables 7 and 8. Also, it was observed from 0.02s to 0.25s the batteries supply the active and reactive power of DSTATCOM, where the active power equal 27KW, and the reactive power approximately equal 5KVAR, and from 0.25s to 0.4s the batteries and PV panels have worked as a hybrid source, and from 0.4s to 0.8s the mode of a high production

power PV panels where it cover the demand load and the same time the batteries charging, and then back to the hybrid mode from 0.8s to 0.9s to supply the load.

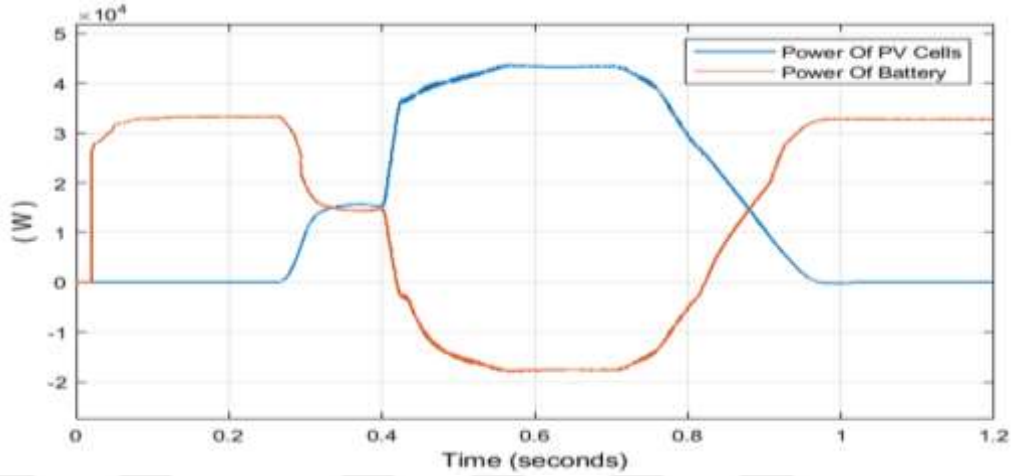

Figure 42. The power of PV panels and power of batteries.

Figure 43 shows the Unity Power Factor (UPF) between the voltage source phase (A) and current source phase (A).

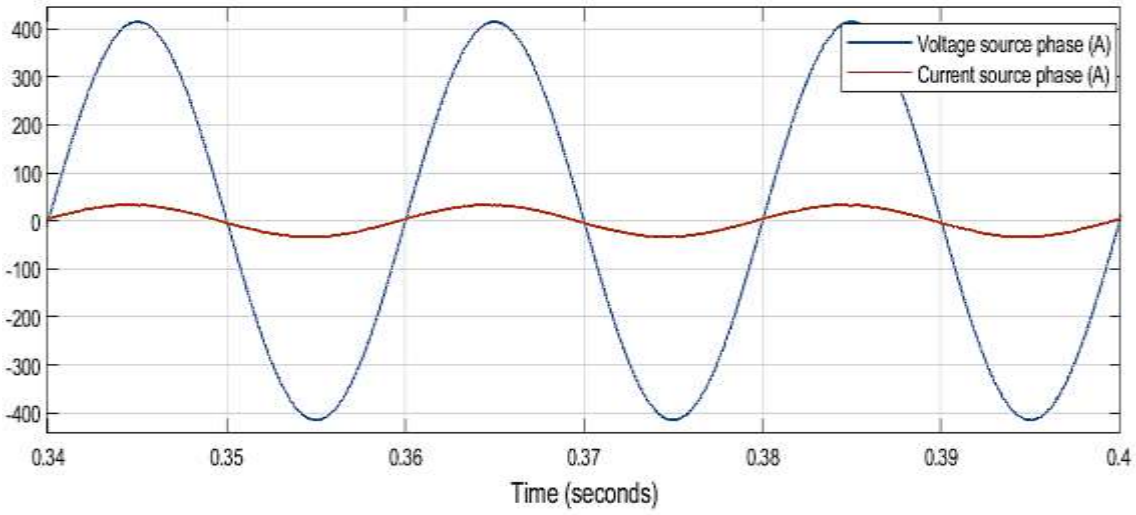

Figure 43. The UPF between voltage and current source of phase (A).

4.2.4 After Compensation with PV System With Arduino Sensors (Real time)

i. Arduino sensors have been used to represent a real-time (radiation and temperature) at daytime:

The reading was taken (radiation and temperature) in the day time (sunny day) at 3 p.m, on day 22-3-2023.

Figure 44 shows in (a, b) the variable radiation and temperature reading that taken from Arduino sensors respectively, (c, d) the voltage and current of the batteries respectively and it is observed the batteries in the charge mode because the sensors working at daytime mode (e) the status of charge and discharge of batteries, and (f) the current supply generator source for phase.A after compensation.

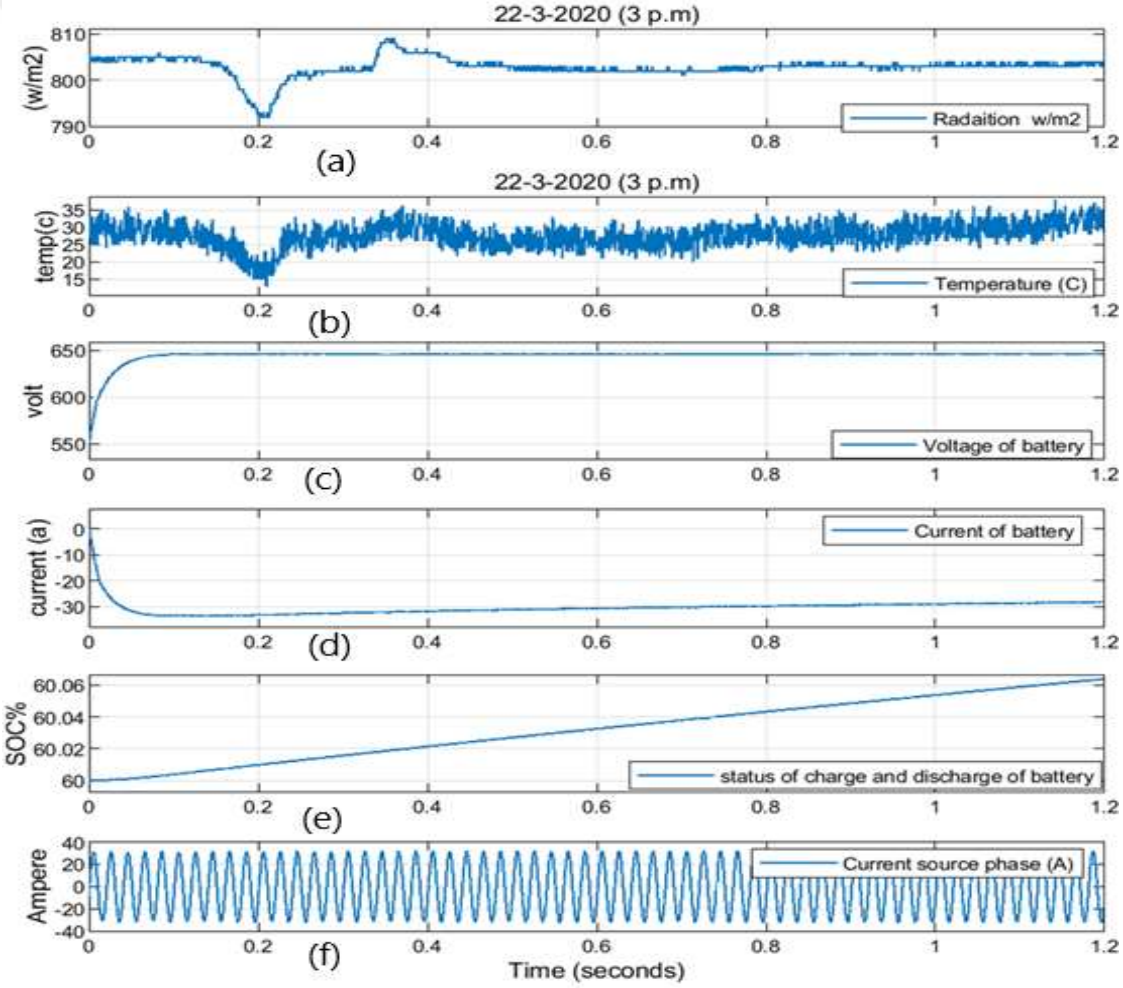

Figure 44. Status for situation Arduino sensors mode.

Figure 45 shows the three phase current of source after compensation and the value of source current equal 32A.

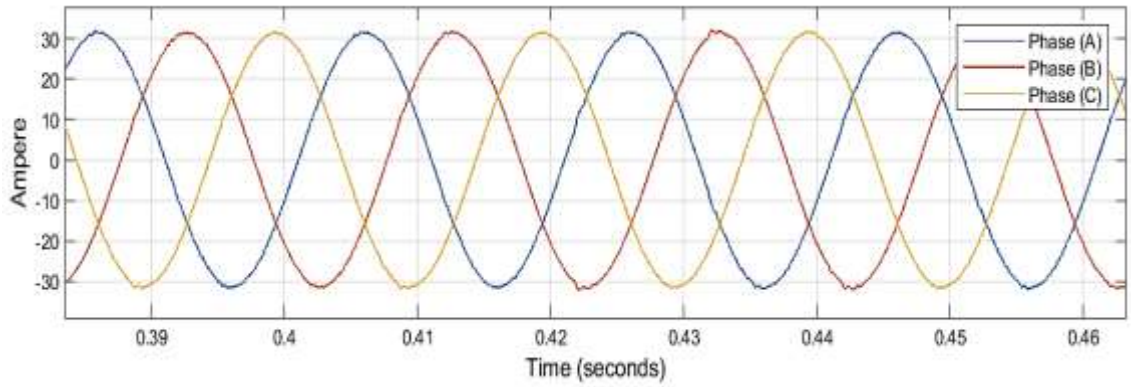

Figure 45. Three phase current for supply source with compensation when used Arduino sensors.

Figure 46: The THD% proportion for three phase current of supply source when using Arduino sensors.

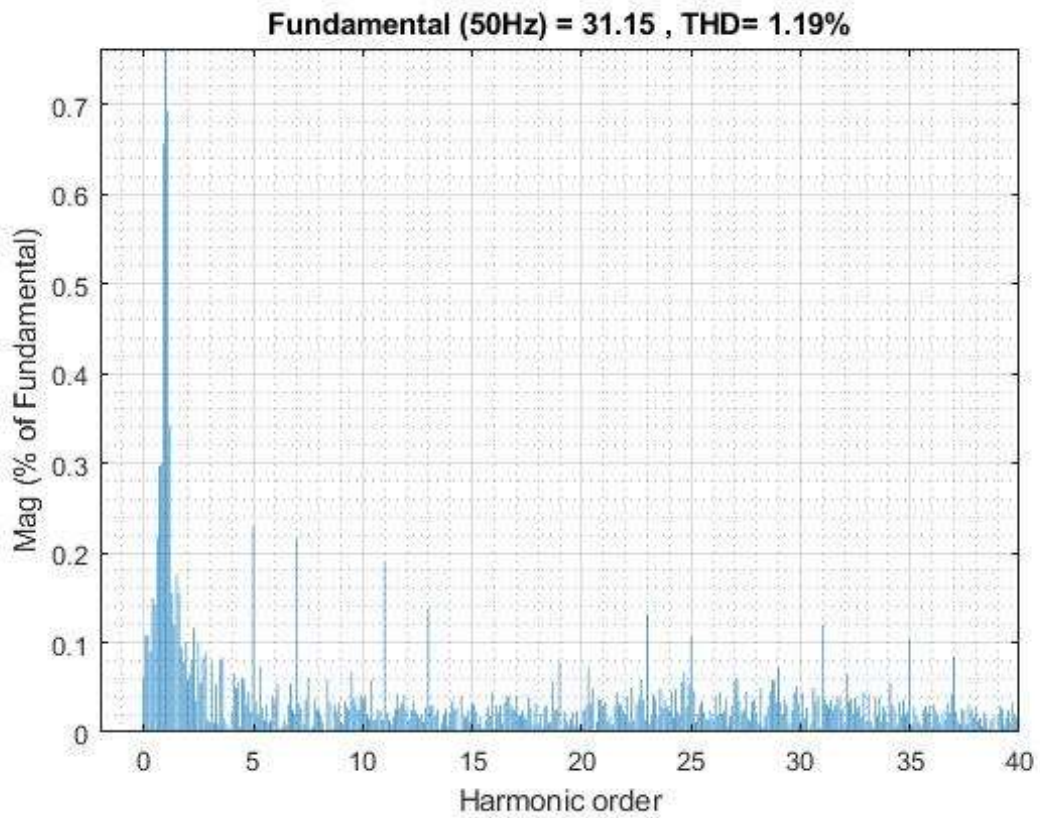

Figure 46. The THD% for three phase current of the supply source after compensation at Arduino sensors.

Figure 47 shows the power of PV cells production when using Arduino sensors on a sunny day at 3p.m, and the production approximately 47.5kW. It observed distribution 32.5kW covered the active power of load demand and the 15kW for charging the batteries.

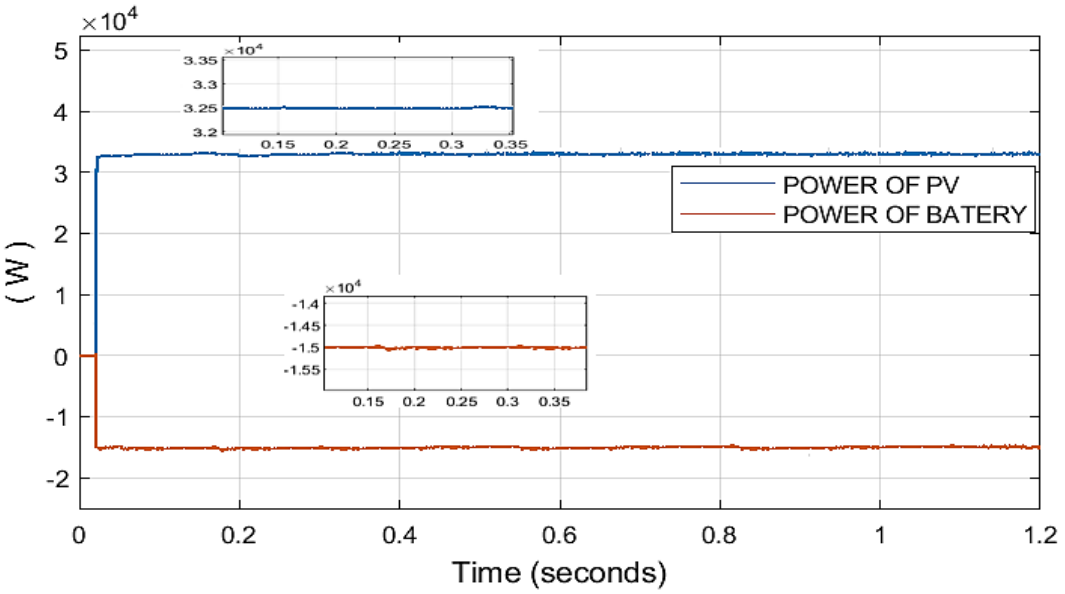

Figure 47. The power production from the PV panels and batteries when using the Arduino sensor.

CONCLUSIONS AND RECOMMENDATIONS FOR FUTURE WORK

- **Conclusions**

For the purposes of this thesis, we used a PV system made up of photovoltaic modules (PV panels) and energy storage (batteries) for individual feeding on the PV panels or batteries or multiple supply sources (PV panels and batteries) combined with high coordination on the dc-channel VSC for DSTATCOM. The purpose of utilizing this technology is to increase the power quality of the electrical system. It is worth noting that the PV system technology in the dc-channel of DSTATCOM has been used for the first time in the compensation systems MatLab/Simulink 2018a.

- **The Part of Work**

The part of work to prove the general idea as pour simulation for the design of the thesis, where two inputs PV panels and Batteries have been proposed for operation of the dc-channel supply that provided a high coordinated logic circuit for the supply of DSTATCOM in order to maintain continual of power throughout the daytime, night-time and cloudy times state through PV panels converter (Boost) and the batteries bi-directional converter circuit (Buck-Boost). After connecting the PV panels and batteries source to the input of dc-channel for DSTATCOM. Also, the three-phase currents of source have been compensated and reduced the total harmonic distortion. A Synchronous Reference Frame with Unit Vector Method (SRFUVM) algorithm has been used to control circuit of DSTATCOM. To obtained the high regulation between PV panels and batteries, the high coordination logical circuit has been used between the PV panels and batteries converters for input of VSC.

The results for present work With Non-linear load.

For each of cases the test has been applied with four situations for PV panels and batteries on the dc-channel link of VSC-DSTATCOM:

iii. Power compensation during the cloudy day-time (cloudy mode).

iv. Power surplus of panels at day-time (high production mode).

v. Arduino sensors have been used to represent a real-time for (radiation and temperature) at day time.

The results of (model) shown:

i- The results of (model) have presented a high performance for the PV system (PV panels and batteries) for multi-renewable dc sources of DSTATCOM in the compensation.

ii- The real time of arduino sensors are provided the real value of irradiation and temperature compare with insert value of (irradiation and temperature).

iii- The results show improving the power quality of the source by reducing the Total Harmonics Distortion (THD%) compare with the literature review for the three phase currents source. As shows in the figer below

iv- The results have been proved the PV panels and batteries can be worked as PVsystem supply sources for the dc-link channel of DSTATCOM voltage source converter (VSC).

v- Comparison with literature review (similar systems)

Table 11 shown the comparison between the present work and other work, As it can be seen, the current work is superior when compared to previous works

Table 11. The compartor between current work and previous work,

Previous work	**THD befor copensation**	**THD after compensation**	**3 Phase current source**
Reference (V Kamatchi Kannan and N Rengarajan, 2012)	27.59%	5.38%	65 A
Reference (Firas, et al,. 2020)	28.9%	1.68%	35 A
Current work	28.25%	1.19%	32 A

- **Recommendations for Future Work**

This work can be further expanded and strengthened in the future, utilizing the following concepts or ideas:

1. Practical Implementation of DSTATCOM with cuttlefish-PI controller utilizing Power Systems Computer Aided Design (PSCAD).
2. It can use other types of the whale algorithm or PSO-GA algorithm to unit training of PI controller for the control circuit of DSTATCOM to obtain the optimal results.
3. This idea can be applied on the unified power flow controller (UPFC).
4. It can use other renewable energies, like wind energy with PV panels (PV panels and Wind), where the solar come in daytime and the most of wind come in the nighttime or (Wind and batteries) or three sources (PV panels, batteries and wind) on the dc-link channel for DSTATCOM or UPFC.

REFERENCES

Agbetuyi, A. F., Orovwode, H., Olowoleni, J. ve Nwangwu, C. (2018). Design and Implementation of a Solar Energy Measurement and Monitoring System. *IEEE Power Engineering Society Conference and Exposition in Africa, Power Africa*, 833-840.

Akhilesh, K. G., Deepak, K., Bandi, M. R., ve Paulson, S. (2017). BBBC based Optimization of PI Controller Parameters for Buck Converter. *i-PACT 2017, Vellore Institute of technology, Vellore, Tamilnadu, India*.

Amirnaser, Y. (2010). Voltage sourced converters in power system Modeling, control, and application. *IEEE WILEY press*.

Amit, K., Pandey, Suchi, S., ve RP, K. (2018). Compensation of neutral current using unit vector template method-based control algorithm for DSTATCOM to power quality improvement. *International Journal of Science Engineering and Technolog*, 6(2), 154-159.

Amit, K., Mukul, A., ve Pradeep, K. (2019). Integration of PV array in DSTATCOM with Comparative Analysis of Different Control Mechanisms. *International Journal of Applied Engineering Research*, 14(2), 169-176.

Arindam, C., Shravana, K. M., Anurag, K. S., ve Anil, K. K. (2012). Integrating STATCOM and Battery Energy Storage System for Power System Transient Stability: A Review and Application. *Advances in Power Electronics*.

Askari, M. B., Mirzaei, M., ve Mirhabibi, M. (2015). Types of Solar Cells and Application. *American Journal of Optics and Photonics*, 3(5), 94-113.

Avjs, P., ve Sheldon, Williamson. (2019). A Wide Input and Output Voltage Range Battery Charger Using Buck-Boost Power Factor Correction Converter. *IEEE Applied Power Electronics Conference and Exposition (APEC)*, 2974-2979.

Bhim, S., Rastgoufard, P., Brij, S., Ambrish, C., ve Al-Haddad, K. (2004). Design simulation and implementation of three pole/four-pole topologies for active filters. *IEE Proceedings-Electric Power Applications*, 151(4), 467-476.

Bina, M. T., ve DC H. (2005). Average Circuit Model for Angle-Controlled STATCOM. *IEE Proceedings on Electrical Power Applications*, 153(3), 653-659.

Binayak, B., Shiva, R. Poudel., Kyung-Tae, L., ve Sung-Hoon, Ah. (2014). Mathematical Modeling of Hybrid Renewable Energy System: A Review on Small Hydro-Solar-Wind Power Generation. *International Journal of Precision Engineering and Manufacturing-Green Technology*, 1(2), 157-173.

Braz, d. J. C. F., Steffen, B., ve Thomas, A. L. (1997). A new control strategy for the PWM current stiff rectifier/inverter with resonant snubbers. *IEEE Power Electronics Specialists Conference*, 2(6), 573-579.

Chi-Seng, L., Man, C. W., Wai-Hei, C., Xiao-Xi C., Hong-Ming, M., ve Jianzheng, Liu. (2014). Design and Performance of an Adaptive Low-DC-Voltage-Controlled LC-Hybrid Active Power Filter With a Neutral Inductor in Three-Phase Four-Wire Power Systems. *IEEE Transactions on Industrial Electronics*, 61(6), 2635-2647.

Chung-Chuan, H., ve Hsin-Ping, Su. (2014). A multi-carrier PWM for AC-DC-AC converter without DC link electrolytic capacitor. *Power Electronics Conference (IPEC).*

Daniel, C. Z., ve Filip, S. (2018). Design of Bidirectional DC/DC Battery Management System for Electrical Yacht. *Thesis in Electrical Engineering*, 12-70.

Deepak, V., Savita, N., Soubhagya, K., ve Soubhagya, K. D. (2015). Maximum power point tracking (MPPT) techniques: Recapitulation in solar photovoltaic systems. *Renewable and Sustainable Energy Reviews*, 54(3), 1018-1034.

Digvijay, K., Arun, T., ve HT l. (2015). Distribution Static compensator for Power Quality Improvement using PV Array. *IEEE International Conference on Electrical, Computer and Communication Technologies (ICECCT).*

Erkan, D., ve Osman, K. (2012). Comparative evaluation of different power management strategies of a stand-alone PV/Wind/PEMFC hybrid power system. *International Journal of Electrical Power & Energy Systems*, 34(1), 81-89.

Fayadh, A., ve Yarab, Aldouri. (2014). Review on the energy and renewable energy status in Iraq: the outlooks. *Renewable and Sustainable Energy*, 39(11), 816-827.

Firas, S. A., Ali, N. H., ve Ahmed, J. Ali. (2020). Power quality improvement by using multiple sources of PV and battery for DSTATCOM based on coordinated design. *Iop Conference Series Materials Science and Engineering*, 745, 1-18.

Georgios, T., ve Georgios, A. (2011). Investigation of the behavior of a three phase grid-connected photovoltaic. *Electric Power Systems Research*, 81(1), 177-184.

Igor, Papic. (2006). Simulation Model for Discharging a Lead-Acid Battery Energy Storage System for Load Leveling. *IEEE Transactions on Energy Conversion*, 21(2), 608-615.

Irena, W., Rozmyslaw, M., Ryszard, P., ve Piotr, G. (2008). Application of DSTATCOM compensators for mitigation of power quality disturbances in low voltage grid with distributed generation. *International Conference on Electrical Power Quality and Utilisation*.

Jan, Z., Petra, S., ve Christin, W. (2008). Public acceptance of renewable energies: Results from case studies in Germany. *Energy Policy*, 36(11), 4136-4141.

Javier, A. K., ve Raul, L. (2004). Model Synthesis for Design of Switched Systems Using a Variable Structure System Formulation. *Journal of Dynamic Systems, Measurement, and Control*, 125(4), 618-629.

Jou H-L, K.-D Wu, J.-C Wu, C.-H Li and M.-S Huang, "Novel power converter topology for three phase four-wire hybrid power filter", IET Power Electronics, Vol. 1, No. 1, PP. 164 -173, 21 March 2008.

Juan Dixon, Luis Moran, Jose Rodriguez, and Ricardo Domke, "Reactive Power Compensation Technologies: State of the Art Review", IEEE Proceedings, Vol. 93, No. 12, PP. 2144-2164, 2005.

Kamatchi, K. V., ve Rengarajan, N. (2012). Photovoltaic based distribution static compensator for power quality improvement. *International Journal of Electrical Power & Energy Systems*, 42(1), 685-692.

Kamatchi, K. V., ve Rengarajan, N. (2014). Investigating the performance of photovoltaic based DSTATCOM using I cosU algorithm. *Electrical Power and Energy Systems*, 54(6), PP. 376-386.

Kavita, K. P., Hareesh, M., Ganjikunta, S. K. (2019). Power Quality Improvement and PV Power Injection by DSTATCOM with Variable DC Link Voltage Control from RSC-MLC. *IEEE Transactions on Sustainable Energy*, 10(2), 1-10.

Kazem, P., ve Meysam, A. (2019). Identification of Internal Defects of Solar Panels Using Equivalent Circuit. *54th International Universities Power Engineering Conference (UPEC).*

Kirubakaran, V., ve Muthu C. Mari. (2014). A Study of Factors Affecting Solar PV Cell through Matlab/Simulink Model. *International Journal of Scientific Research*, 1(3), 21-25.

Laguado, M. A., Luna-Paipa, E. A., Bustos-Marquez, L. F., ve Sepulveda-Mora, S. B. (2019). Performance comparison between PWM and MPPT charge controllers. *IEEE Transactions on industrial electronics*, 24(1), 6-11.

Maan, J. Buni., Ali, A. A., ve Kadhem. (2018). Effect of solar radiation on photovoltaic cell. *International Research Journal of Advanced Engineering and Science*, 3(3), 47-51.

Majid, A. M., ve Mansour, O. (2014). SCAD/EMTDC based Modeling and Analysis of Power Quality of Variable Speed Wind Turbine with STATCOM or SVC. *International Journal of Enhanced Research in Science Technology & Engineering*, 3(7), 328-339.

Marcelo, G. M., ve PE, M. (2006). Control Design and Simulation of DSTATCOM with Energy Storage for Power Quality Improvements. *IEEE/PES Transmission & Distribution Conference and Exposition: Latin America*, 1-6.

Marcelo, M., ve Pedro, M. (2008). Dynamic Modeling and Control Design of DSTATCOM with Ultra-Capacitor Energy Storage for Power Quality Improvements. *IEEE/PES Transmission & Distribution Conference and Exposition: Latin America*, 1-8.

Metin, K., ve Engin, O. (2011). Synchronous-Reference-Frame-Based Control Method for UPQC Under Unbalanced and Distorted Load Conditions. *IEEE Transactions on Industrial Electronics*, 58(9), 3967-3975.

Muhammad, H. R. (2011). Power Electronics Handbook. *Devices Circuits and Application, 3rd edition. Burlington, MA, USA: Elsevier*.

Mukhtiar, S., Vinod, K., Ambrish, C., ve Rajiv, K. V. (2011). Grid interconnection of renewable energy sources at the distributionl level with power quality improvement features. *IEEE Trans. Power Delivery*, 26(1), 307-315.

Naeem, F. H., Khoraminia, R., ve Seyed, H. H. (2009). Optimization of PI coefficients in DSTATCOM nonlinear controller for regulating DC voltage using Genetic Algorithm. *IEEE Conference on Industrial Electronics and Applications*, 2291-2296.

Om, P. M., ve Abdul, G. S. (2016). Power quality improvement in distribution network using DSTATCOM with battery energy storage system. *Electrical Power and Energy Systems*, 83(4), 229–240.

P, B. (2013). Power Quality Improvement by using DSTATCOM. *International Journal of Emerging Trends in Electrical and Electronics (IJETEE)*, 4(2), 1-14.

Pallavee, B., ve Nema, R. (2013). Maximum power point tracking control techniques: State-of-the-art in photovoltaic applications. *Renewable and Sustainable Energy Reviews*, 23(2), 224-241.

Parimal, B., Archana, T., ve Samruddhi, S. (2014). Modeling and Simulation of STATCOM", *International Journal of Engineering Research & Technology (IJERT)*, 12(3), 200-203.

Paul, K., Oleg, W., cott, S., ve teven, P. (2013). Analysis of electric machinery and drive systems. *3nd edition, United states: IEEE press and Wiley Interscience*.

Rajiv, K. V., Shah, Arifur, R., ve Tim, V. (2015). New Control of PV Solar Farm as STATCOM (PV-STATCOM) for Increasing Grid Power Transmission Limits During Night and Day. *IEEE Transactions on Power Delivery*, 30(2), 755-763.

Rajiv, V., ve Reza, S. (2017). SSR Mitigation with a New Control of PV Solar Farm as STATCOM (PV-STATCOM). *IEEE Transactions on Sustainable Energy*, 8(4), 1473-1483.

Ramon, G., Emesto, V., Charmaine, P., ve Arnold, P. (2018). Design and implementation of a DC-DC boost converter for continuous hybrid power system. *IEEE International Conference on Humanoid, Nanotechnology, Information Technology, Communication and Control, Environment and Management (HNICEM).*

Reyes, H., ve Patricio, S. (2009). Instantaneous Reactive Power Theory: A Reference in the Nonlinear Loads Compensation. *IEEE Transactions on Industrial Electronics*, 56(6), 2015-2022.

Safari, A., ve Mekhilef, S. (2011). Incremental Conductance MPPT Method for PV Systems. *Canadian Conference on Electrical and Computer Engineering (CCECE)*.

Salah, T., Nabil, B., Toufik, R., Djamila, R., ve Rachid, A. (2015). Wind turbine-DFIG/photovoltaic/fuel cell hybrid power sources system associated with hydrogen storage energy for micro-grid applications. *In Proceedings of IEEE International Renewable and Sustainable Energy Conference, IRSEC*.

San, N. K., ve Zaw, Tun. (2018). Sensor Analysis and Application of Arduino based Temperature and Light Intensity Control for Smart Home System. *International Journal of Scientific and Research Publications*, 8(6), 89-94.

Sarina, A., ve Fangxing. (2014). Coordinated V-f and P-Q Control of Solar Photovoltaic Generators with MPPT and Battery Storage in Microgrids. *IEEE Transactions on Smart Grid*, 3(5), 1270-1281.

Schauder, C., ve Mehta, H. (1993). Vector Analysis and Control of Advanced Static Var Compensator. *IEE Proc C*. 140(4), 299-306.

Shaik, M, M., Gulam, A., Syed, M. M. M., ve Preeti, K. (2016). Power quality improvement using a novel D-STATCOM-control Scheme for Linear and non-linear loads. *International Conference on Electrical, Electronics, and Optimization Techniques (ICEEOT)*, 2147-2153.

Shih-Kuen, C., Tsorng-Juu, L., ve Jiann-Fuh, Chen. (2010). Novel high step-up DC–DC converter for fuel cell energy conversion system. *IEEE Transactions on Industrial Electronics*, 57(6), 2007-2017.

Shusmita, R., Nadia, S. O., ve Quazi, A. M. (2012). Design of a Charge Controller Circuit with Maximum Power Point Tracker (MPPT) for Photovoltaic System. *Thesis submitted to BRAC University*, 24-28.

Siti, A. J., ve Mohamad, H. O. (2018). Solar Energy Measurement Using Arduino. *Malaysia Technical Universities Conference on Engineering and Technology (MUCET)*, 1-6, 23.

Tabatabaei, N. M., Abbasi, S., Boushehir, N.S., ve Jafari, A. (2015). OVERVIEW OF STATCOM TECHNOLOGY. *International Journal on Technical and Physical Problems of Engineering*, 7(2), 23-28.

Widjaja, I., Kumia, K. S., ve Divan. (1995). Switching dynamics of IGBTs in soft-switching converters. *IEEE Transactions on Electron Devices*, 42(3), 445-454.

Zhiping, Y. C., Lingli, Z., ve Mariesa, L. (2001). Integration of a StatCom and Battery Energy Storage. *IEEE Transactions On Power Systems*, 16(2), 254-260.